Di-boson Production and Polarization Measurements with the ATLAS and CMS Detectors

Xuan YANG
Institute of High Energy Physics, CAS

On behalf of the ATLAS and CMS Collaborations

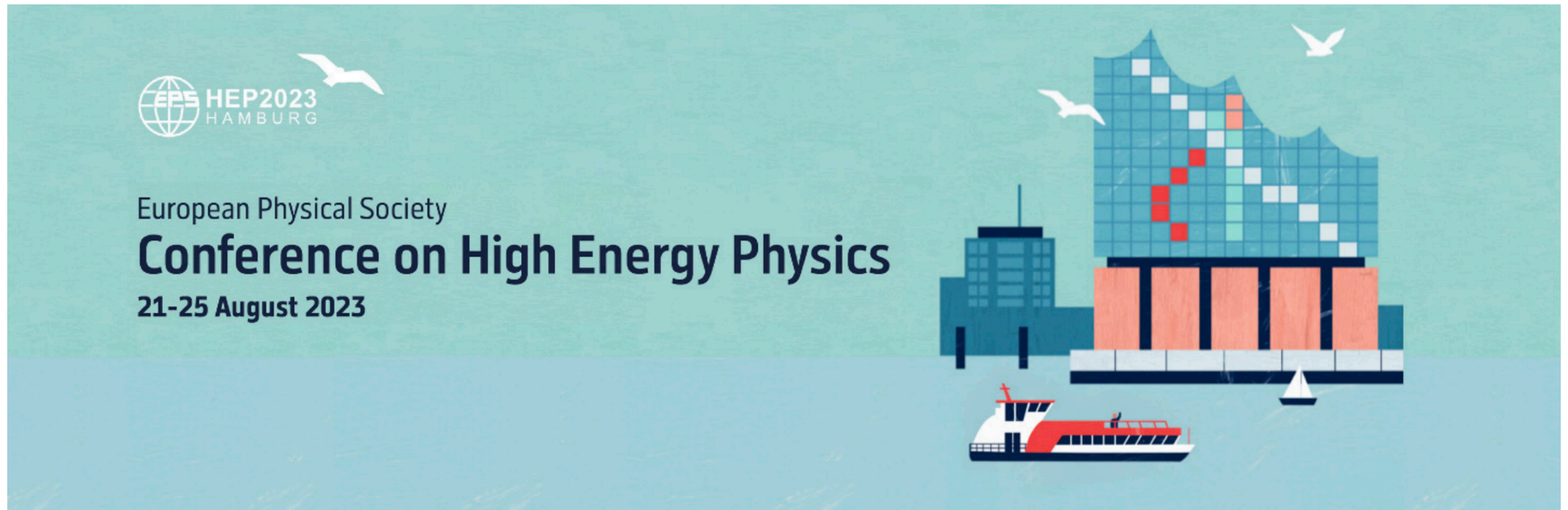

Overview

- Important to probe vector boson couplings in the Standard Model through EWK vertex
  - Sensitive to new physics through anomalous couplings, EFT interpretations
- Indirect test of Higgs mechanism, mass of W/Z boson given by Higgs boson
  - Longitudinal polarization of W/Z boson given by the Higgs mechanism
- Test of fix-order perturbative QCD (pQCD) calculations, Parton shower effect through jet activities
- Included topics:
  - no-VBS production of WW, ZZ, WZ and Zγ results
  - Dedicated talks concerning vector boson scattering production/Triboson production on Wednesday

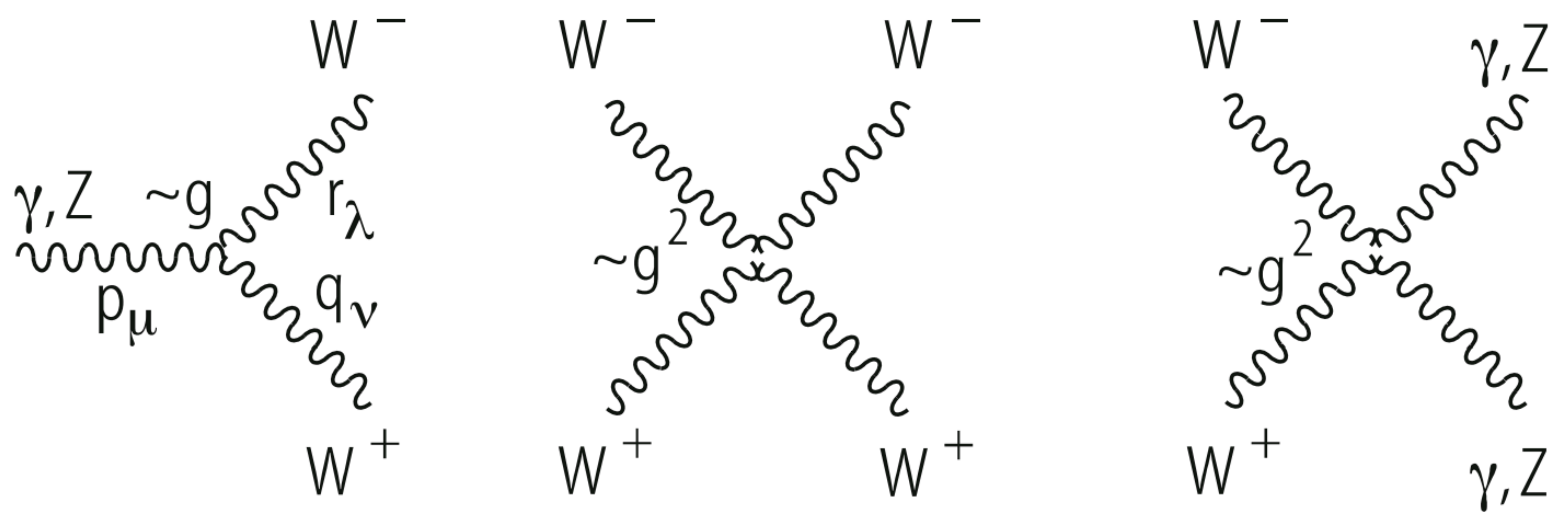

Triple Gauge Boson Coupling and Quartic Gauge Boson Coupling in the SM

W+W- Jet Inclusive

ATLAS-CONF-2023-012

- Fully leptonic final state: $W^+W^- \to e\nu\mu\nu$
- Clear signal, large statistics
- Large backgrounds from ttbar production
- First precision measurement in jet inclusive phase space!

- Top quark background reduced by vetoing b-tagged jets
- Drell-Yan background suppressed by requiring $m_{e\mu}$ > 85 GeV

Dedicated new data-driven method to estimate top quark events -> enabling precision mesurements!

1. Measure $N^{t\bar{t}}_{1b}, N^{t\bar{t}}_{2b}$ in 1-b-jet and 2-b-jet control region
2. Parametrize $t\bar{t}$ events in CR and SR using:
   i. Total events yields: $N^{t\bar{t}}_{\geq 0b}$
   ii. B-tagging efficiency and acceptance: ε_b
   iii. B-jet correlation factor: C_b
3. $N^{t\bar{t}}_{0b} = \frac{C_b}{4}\frac{(N^{t\bar{t}}_{1b} + 2N^{t\bar{t}}_{2b})^2}{N^{t\bar{t}}_{2b}} - N^{t\bar{t}}_{1b} - N^{t\bar{t}}_{2b}$

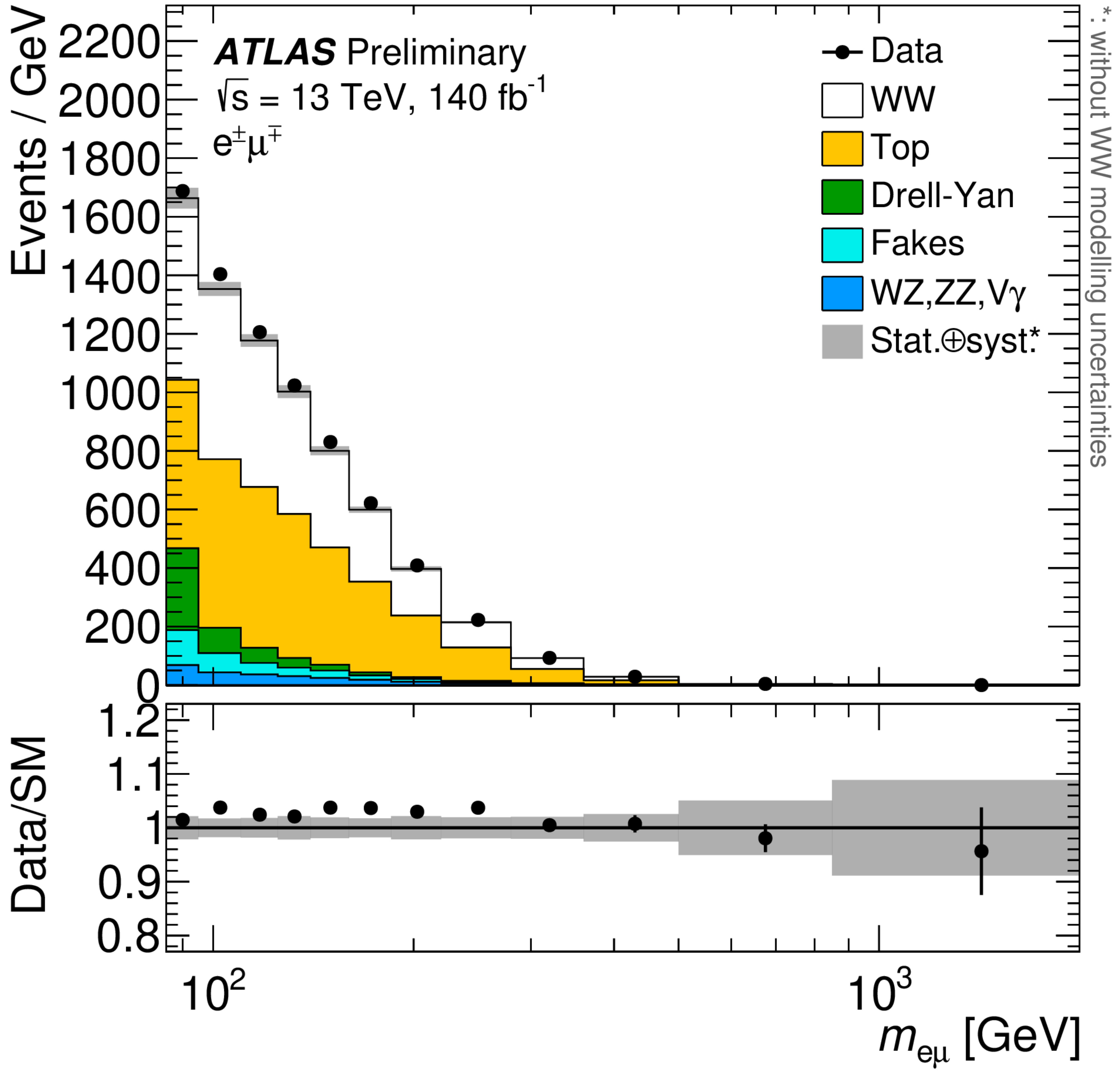

W+W- Jet Inclusive

ATLAS-CONF-2023-012

- Fiducial and differential cross section measured
  - Fiducial XS measured by likelihood fit, extended to full phase space
  - Differential XS measured for 12 observables
- Total uncertainty of 3.1%, dominated by Top modeling and fake background

Uncertainty source	Effect
Total uncertainty	3.1%
Stat. uncertainty	1.1%
Top modelling	1.6%
Fake lepton background	1.5%
Flavour tagging	0.7%
Other background	0.9%
Signal modelling	1.0%
Jet calibration	0.6%
Luminosity	0.8%
Other systematic uncertainties	0.9%

Nice agreement comparing to theoritical predictions!

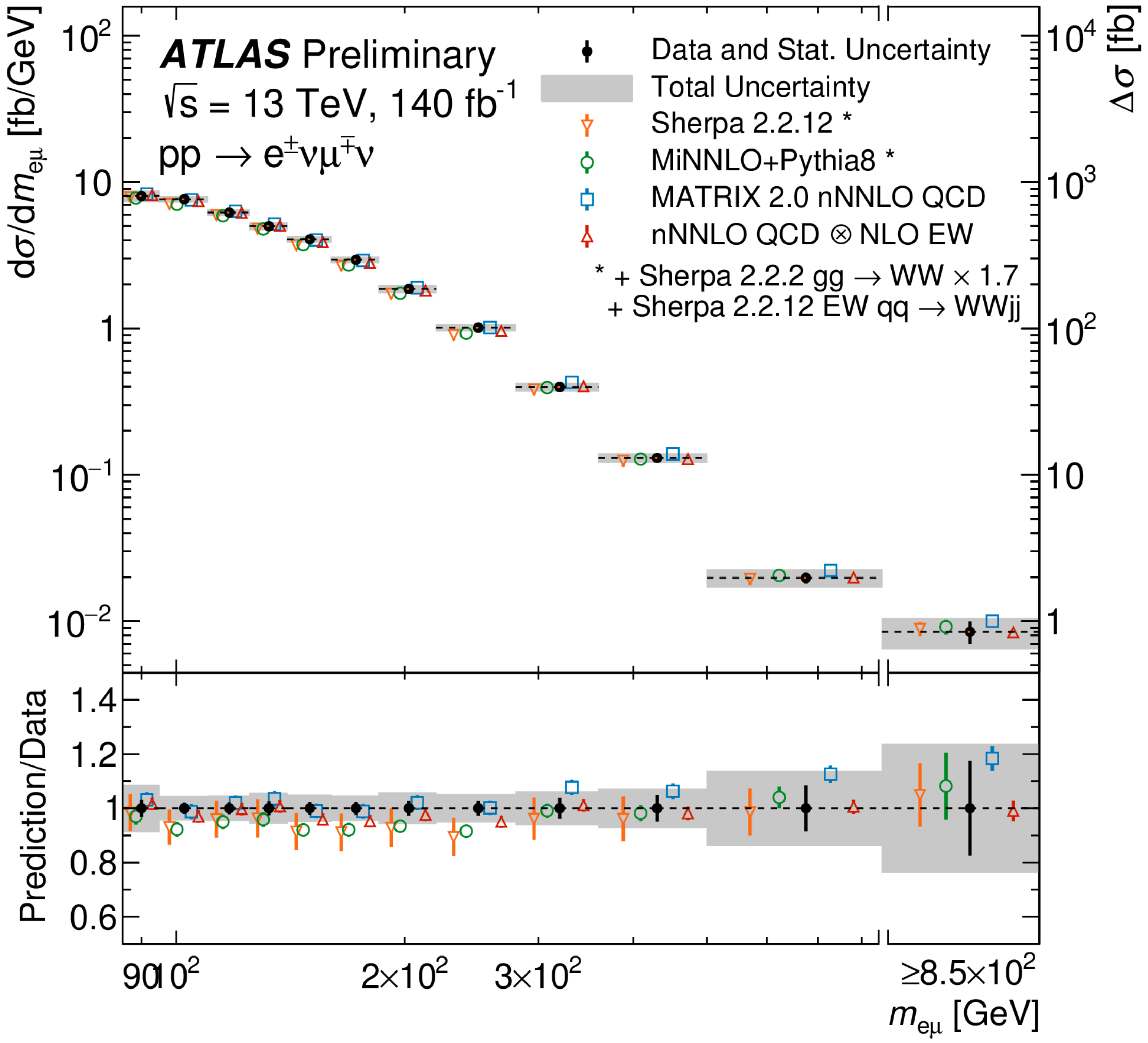

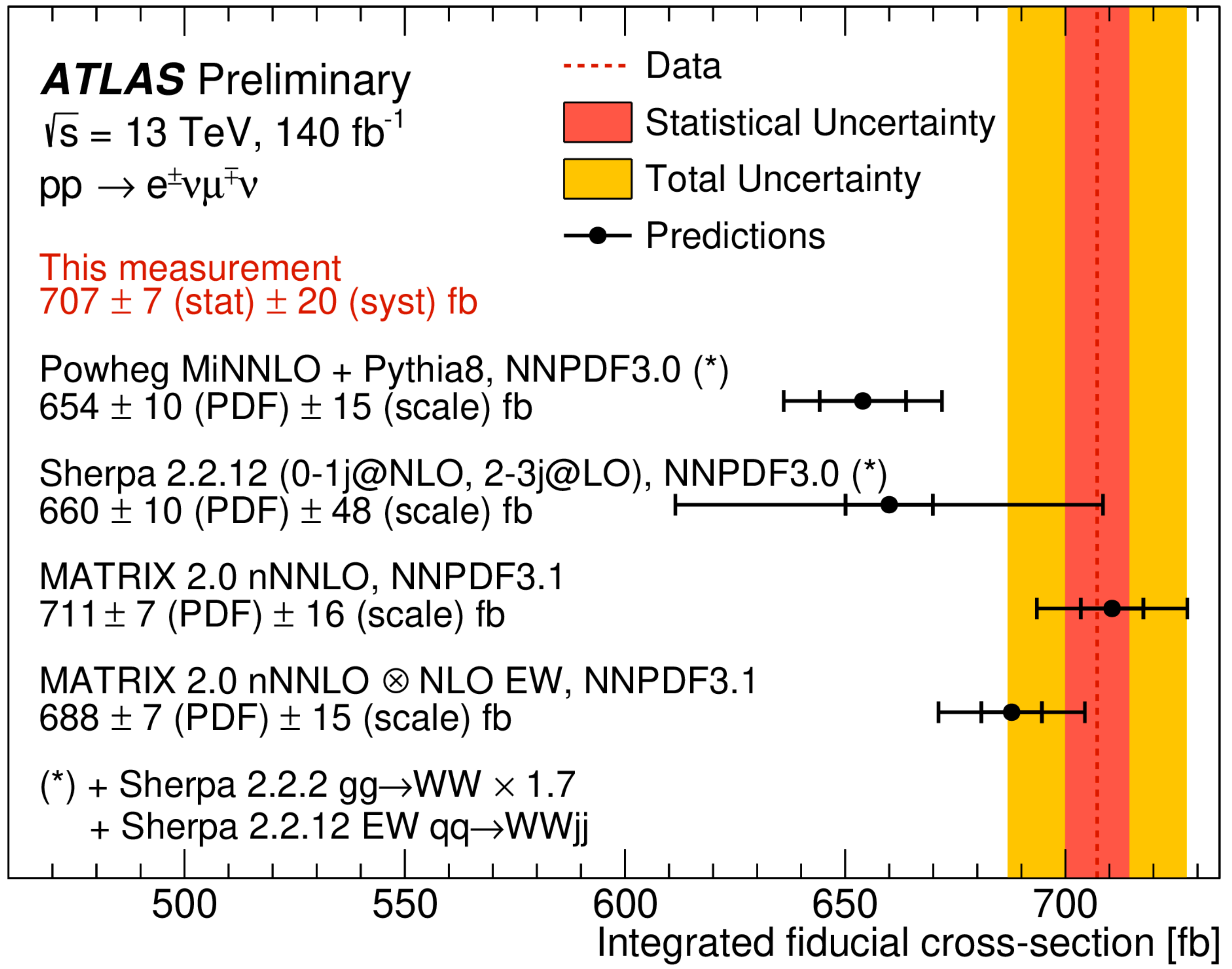

WZ Production Measurement

CMS-SMP-20-014

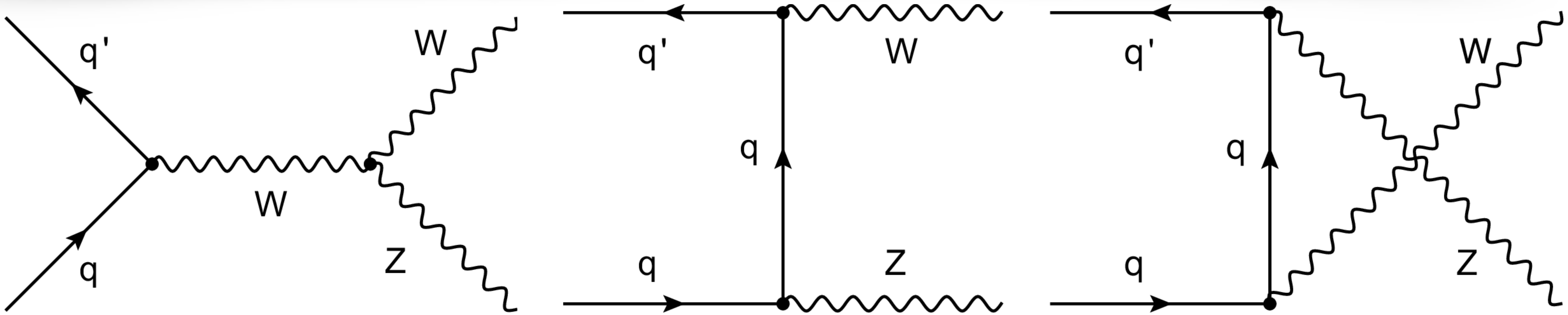

- Electroweak process, sensitive to PDF of quarks
- Fully leptonic final state $WZ \to l\nu ll$, clear signal
- Charge asymmetry $\sigma_{W+Z}/\sigma_{W-Z}$ measurement
- W boson polarization measurements
- Observation of longitudinal polarized W boson in WZ production!
- Fiducial and differential XS measured as functions of sensitive observables   Listed in backup
- Constrain on AGC EFT parameters

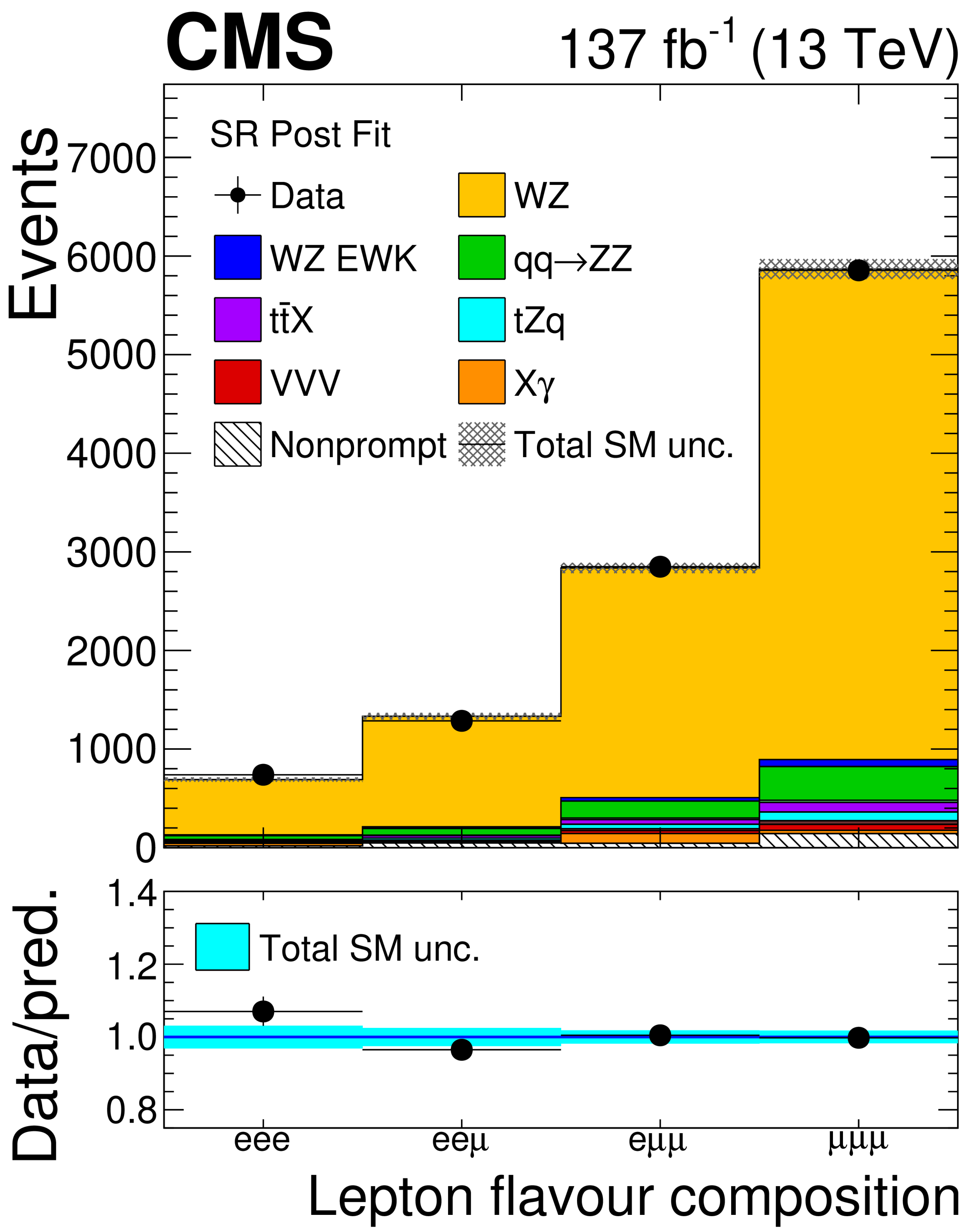

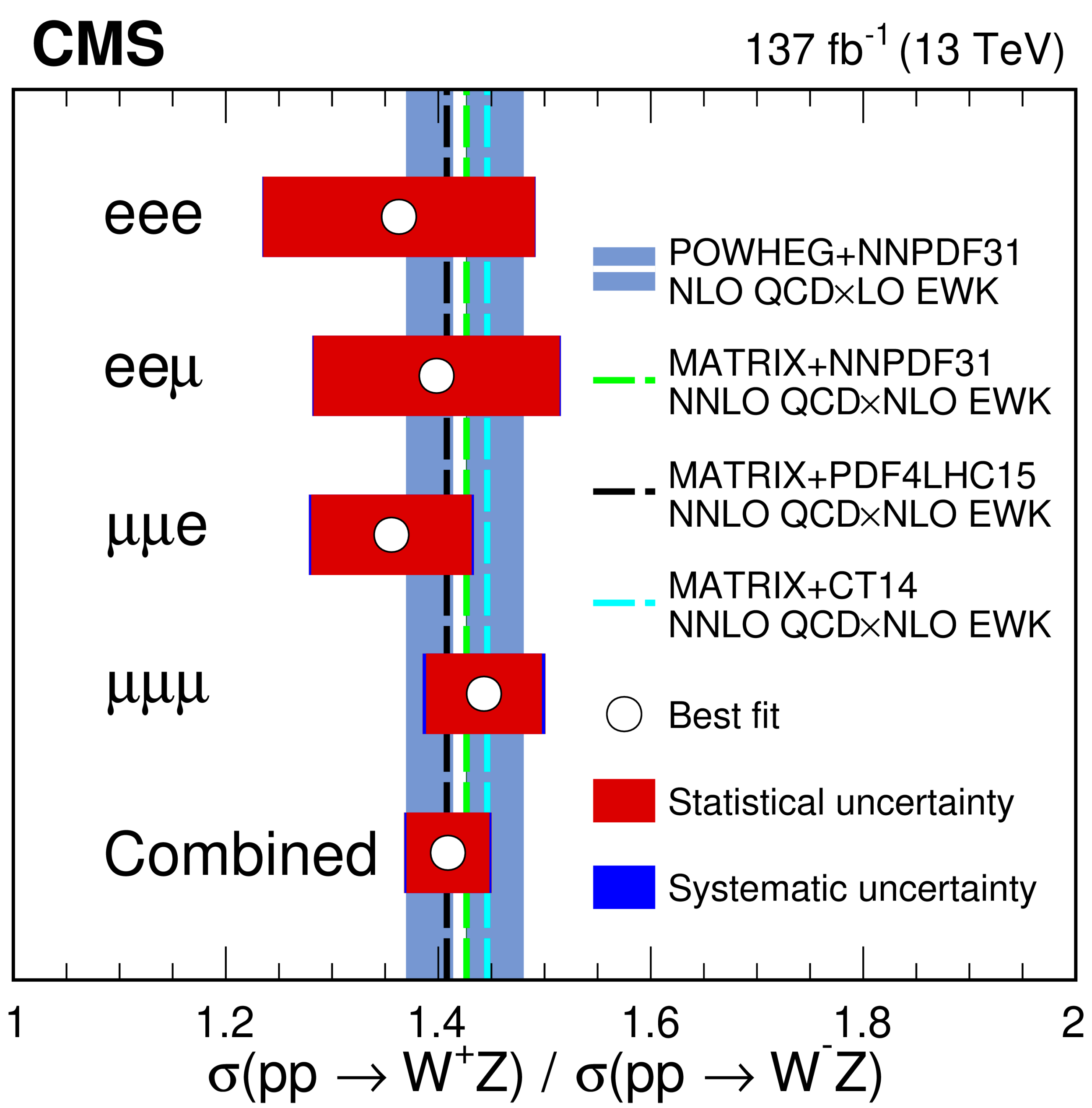

WZ Production Measurement

CMS-SMP-20-014

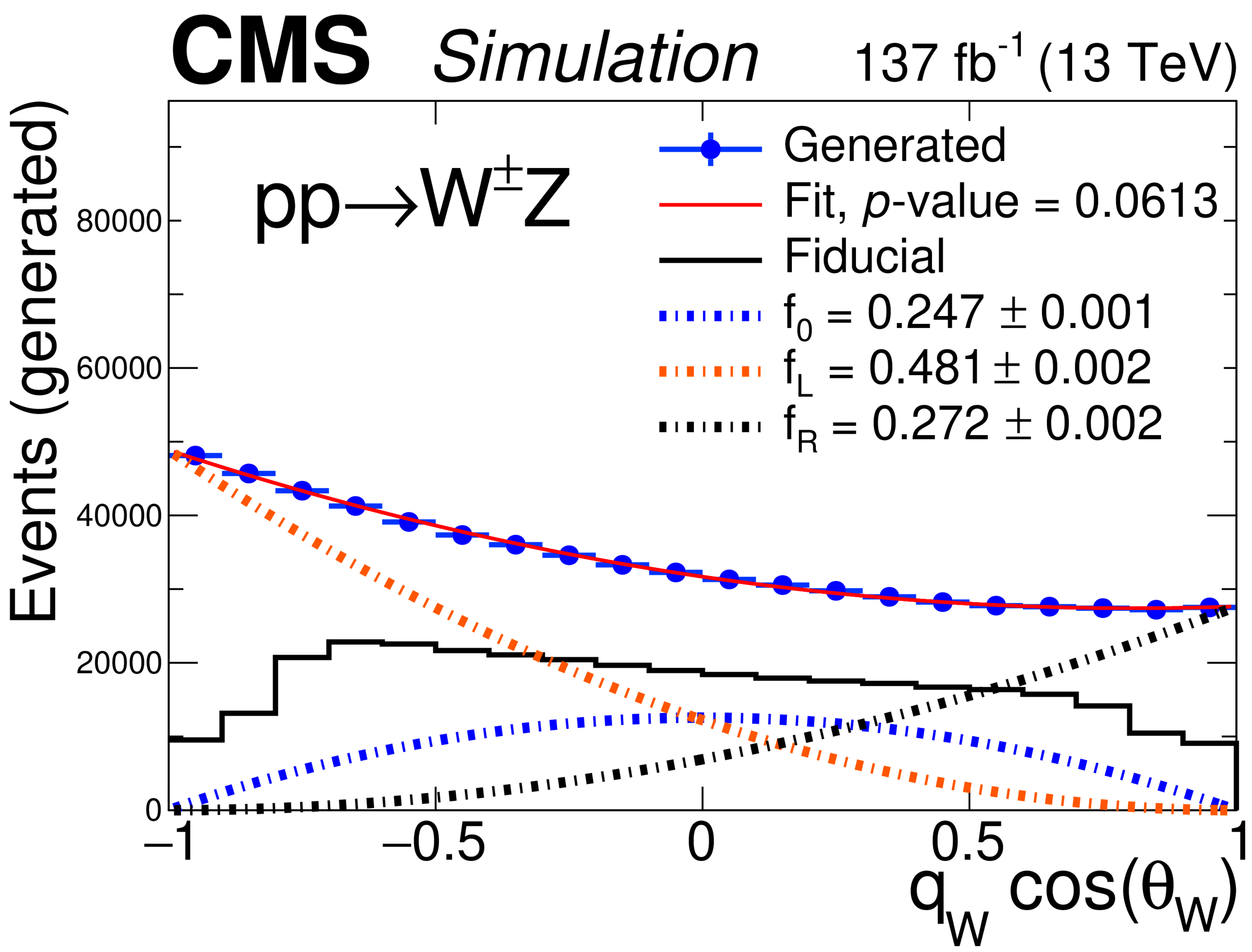

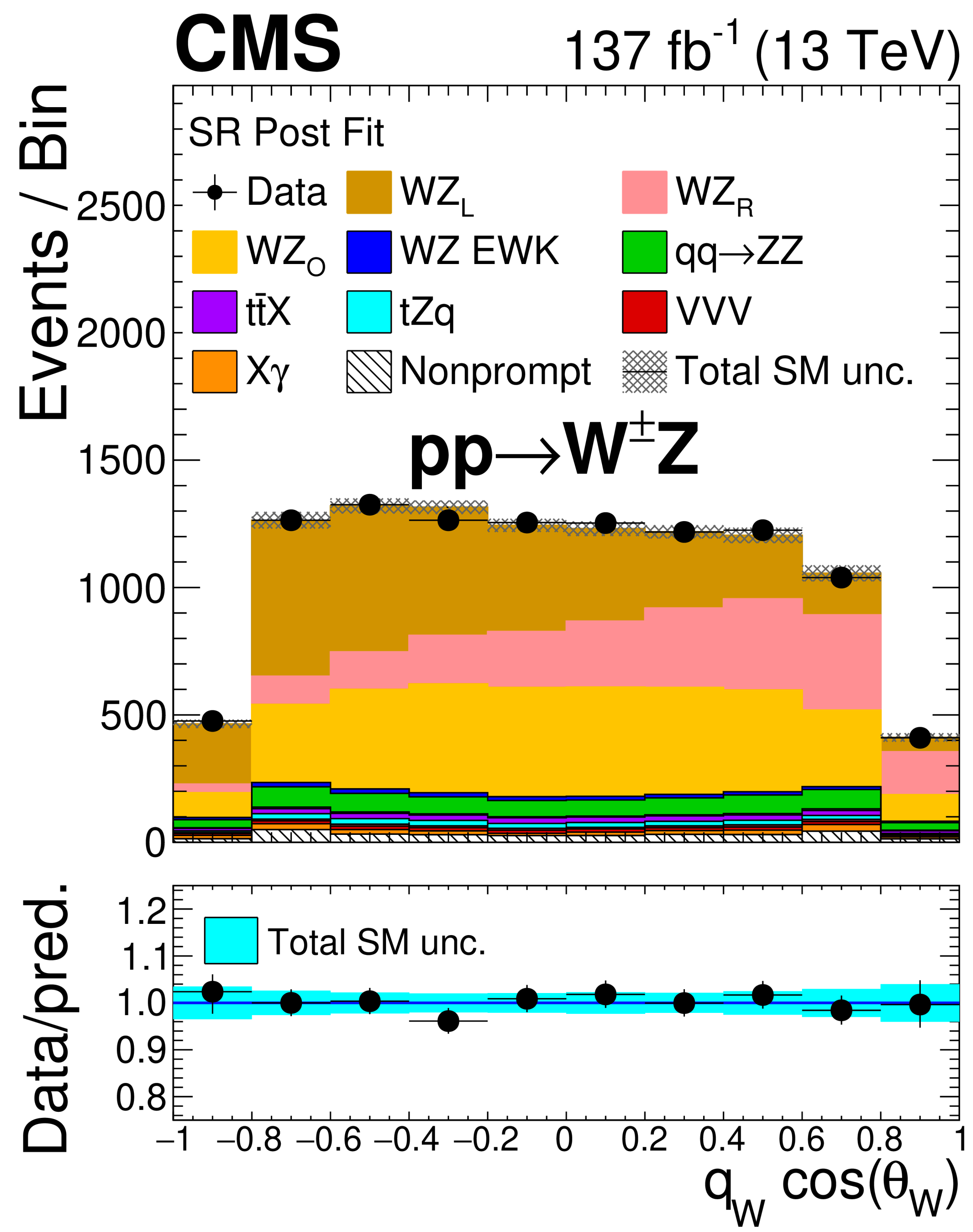

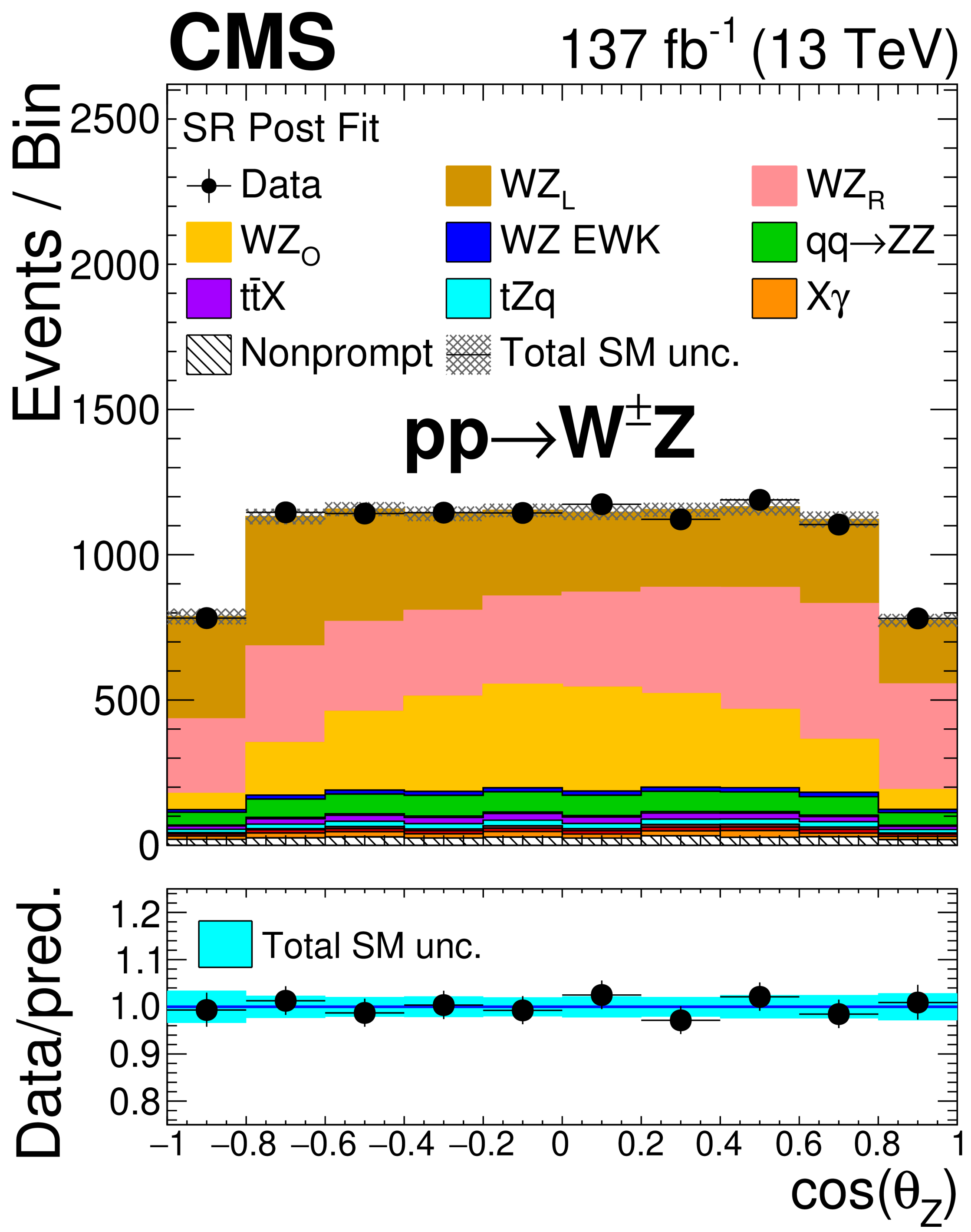

- Templates built for each cosine of polarization angles of W(Z) boson
  - 6 templates in total, including inclusive charge, positively charged and negatively charged W boson
- Likelihood fit to data to extract polarization fraction
  - Longitudinal Z boson observed with a high significance
  - Longitudinal W boson observed with significance of 5.6σ *obs* (4.3σ *exp*)

WZ Joint Polarization

Phys. Lett. B 843 (2023) 137895

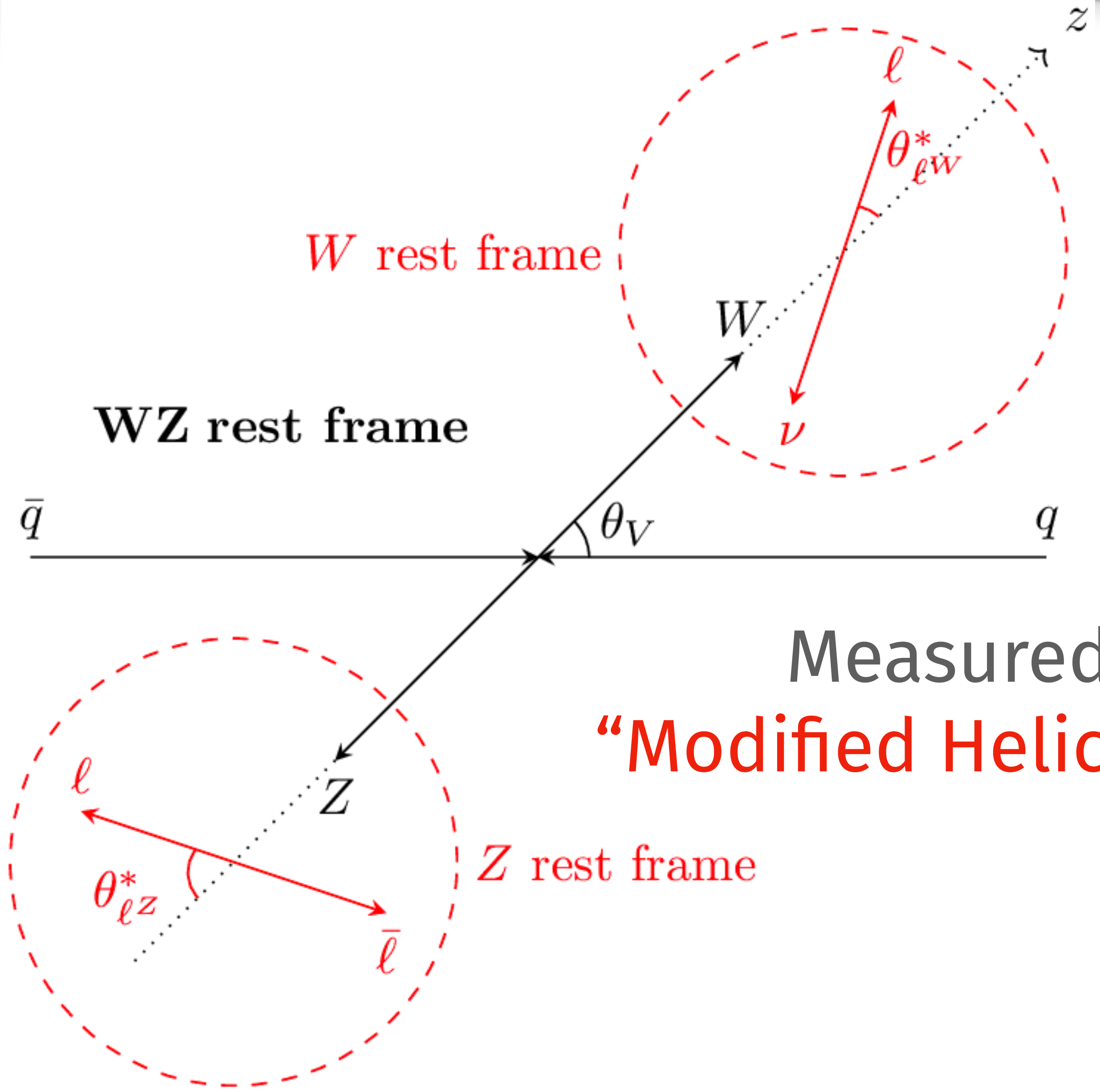

Measured in WZ rest frame

"Modified Helicity Coordinate System"

Decay angle of leptons defined in W(Z) rest frame

$$\rho_{\lambda_W \lambda'_W \lambda_Z \lambda'_Z} \equiv \frac{1}{C} \times \sum_{\mu_q \mu_{\bar{q}}} F^{(\mu_q \mu_{\bar{q}})}_{\lambda_W \lambda_Z} F^{(\mu_q \mu_{\bar{q}})*}_{\lambda'_W \lambda'_Z} \;, \text{where} \quad C = \sum_{\mu_q \mu_{\bar{q}} \lambda_W \lambda_Z} \left| F^{(\mu_q \mu_{\bar{q}})}_{\lambda_W \lambda_Z} \right|^2$$

$$\begin{aligned} f_{00} &= \rho_{0000} \,, \\ f_{\mathrm{TT}} &= \rho_{++--} + \rho_{--++} + \rho_{----} + \rho_{++++} \,, \\ f_{0\mathrm{T}} &= \rho_{00--} + \rho_{00++} \,, \\ f_{\mathrm{T}0} &= \rho_{--00} + \rho_{++00} \,. \end{aligned}$$

Helicity fraction definition in this measurement

4 categories defined by the two angular variable

Use dedicated DNN to separate the four combinations

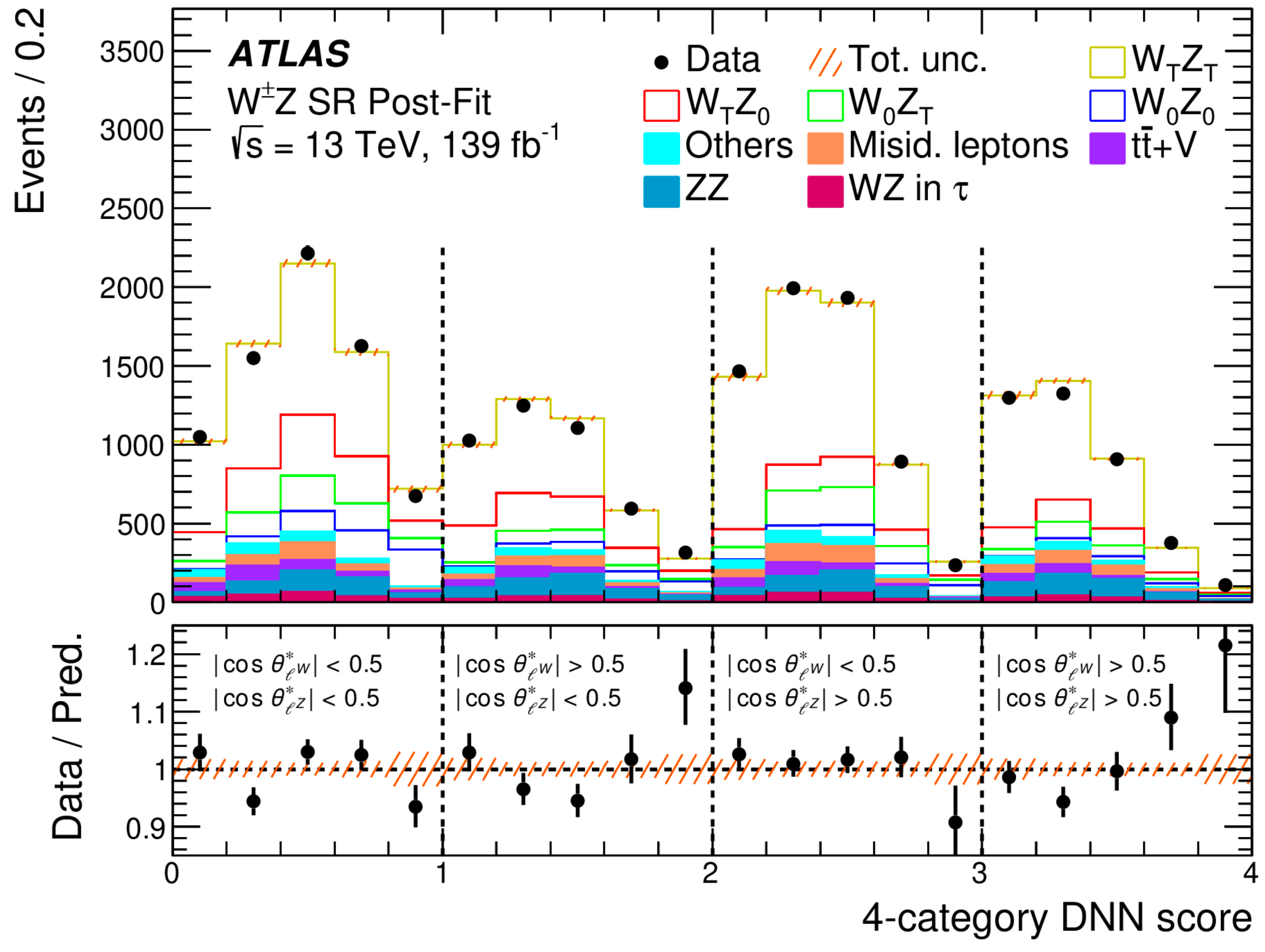

WZ Joint Polarization

Phys. Lett. B 843 (2023) 137895

- Joint polarization measured by binned profile-likelihood fit to the DNN
- First observation of f_{00} state with significance of $7.1\sigma\ obs\ (6.2\sigma\ exp)$
  - $f_{0T}: 3.4\sigma\ (5.4\sigma), f_{T0}: 7.1\sigma\ (6.6\sigma), f_{TT}: 11\sigma\ (9.7\sigma)$
- Compared to theoretical prediction with good agreement

$$f_{00}: 0.067 \pm 0.010\ (Data)\ ,\ 0.058 \pm 0.002\ (NLO\ QCD)$$

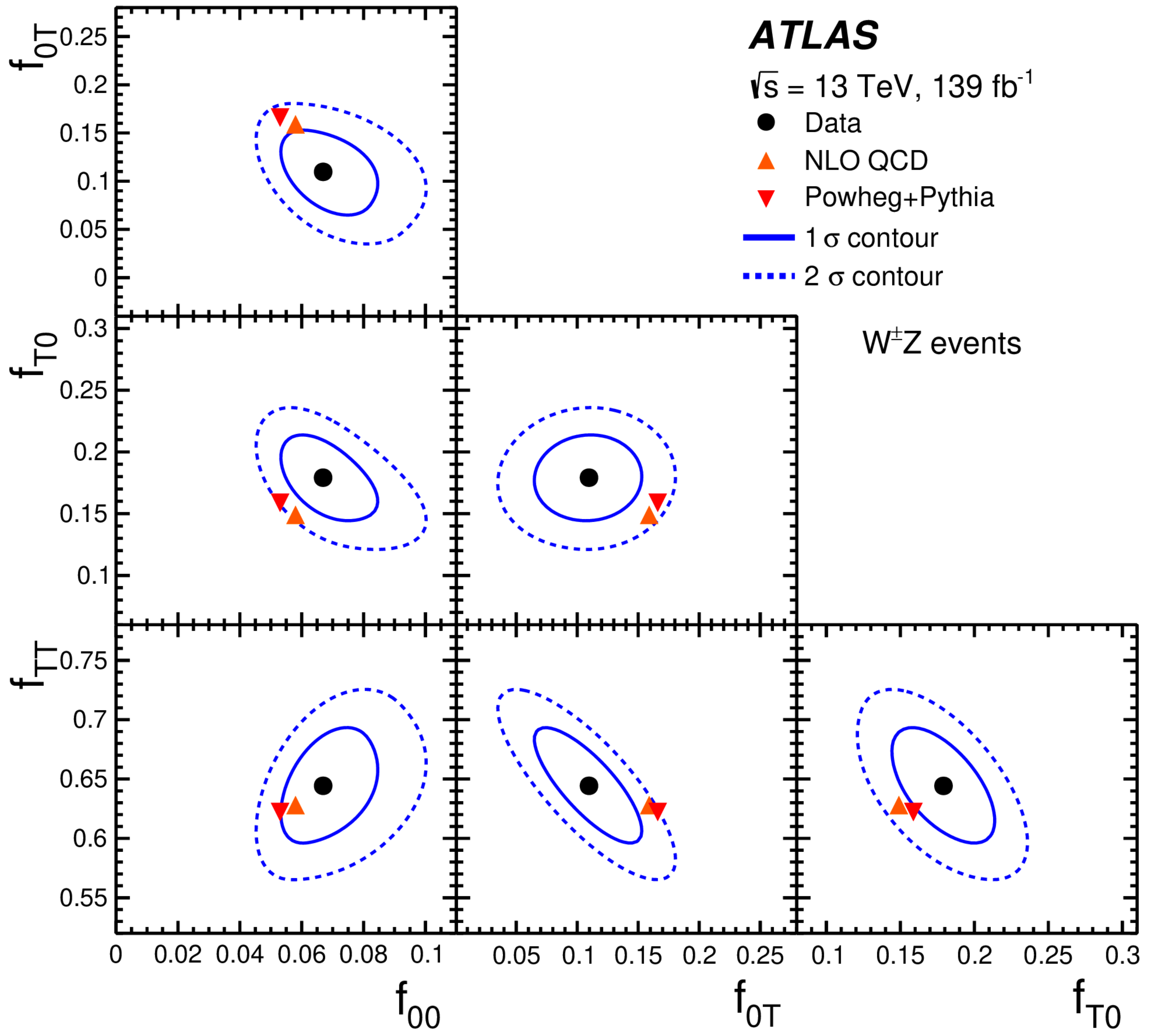

Individual polarization measured by fit on decay angle template built by reweighing

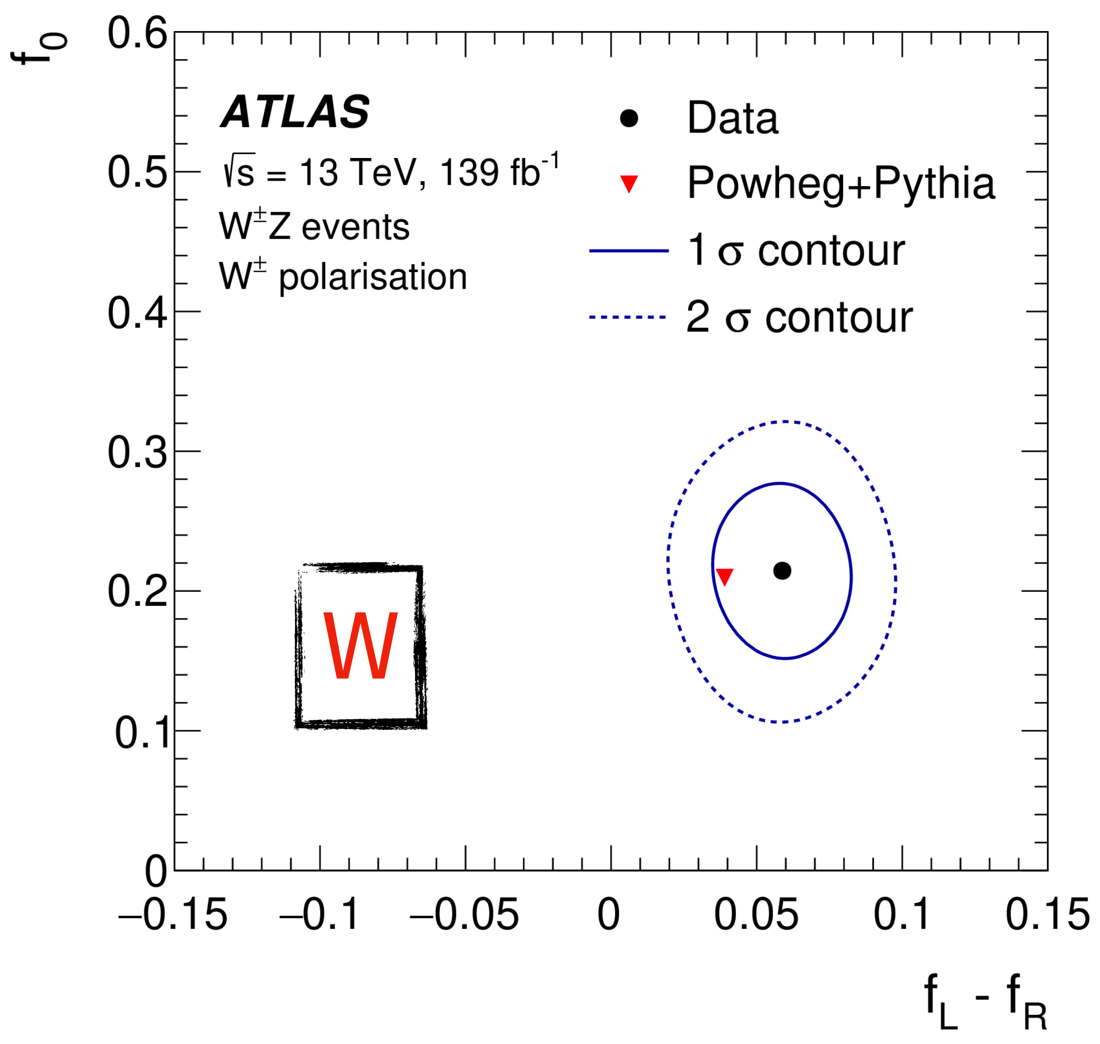

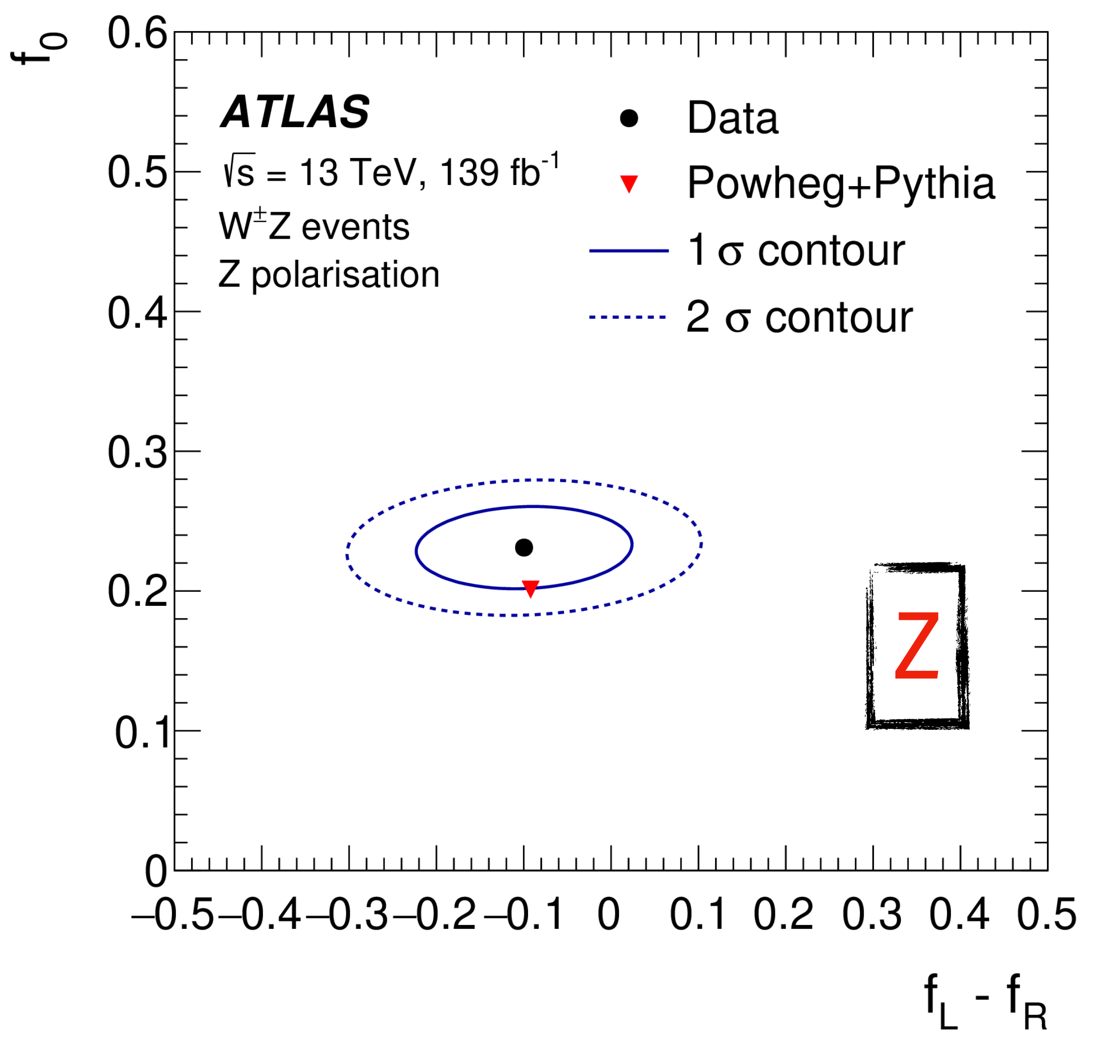

Inclusive XS of WZ production also measured:

$$\sigma^{fid}_{W^\pm Z\to l\nu ll} = 64.6 \pm 0.5\ (stat.)\ \pm 1.8\ (syst.)\ \pm 1.1\ (lumi.)\ fb$$

Differential XS of several kinematics sensitive to polarization are also measured (see backup)

Zγ+Jets Differential

JHEP 07 (2023) 072

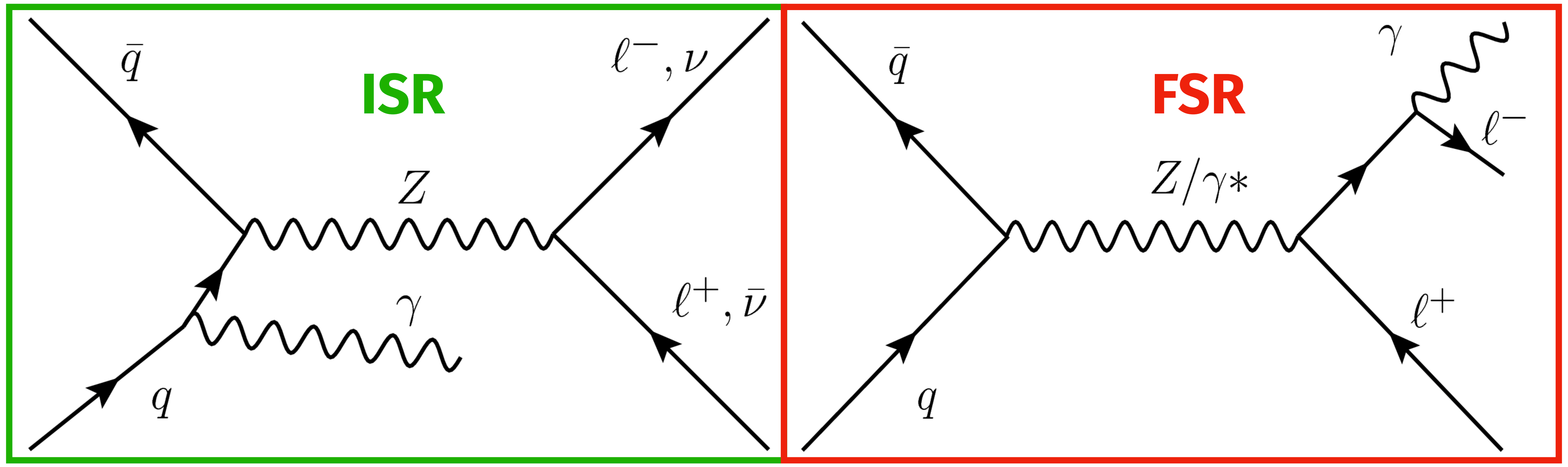

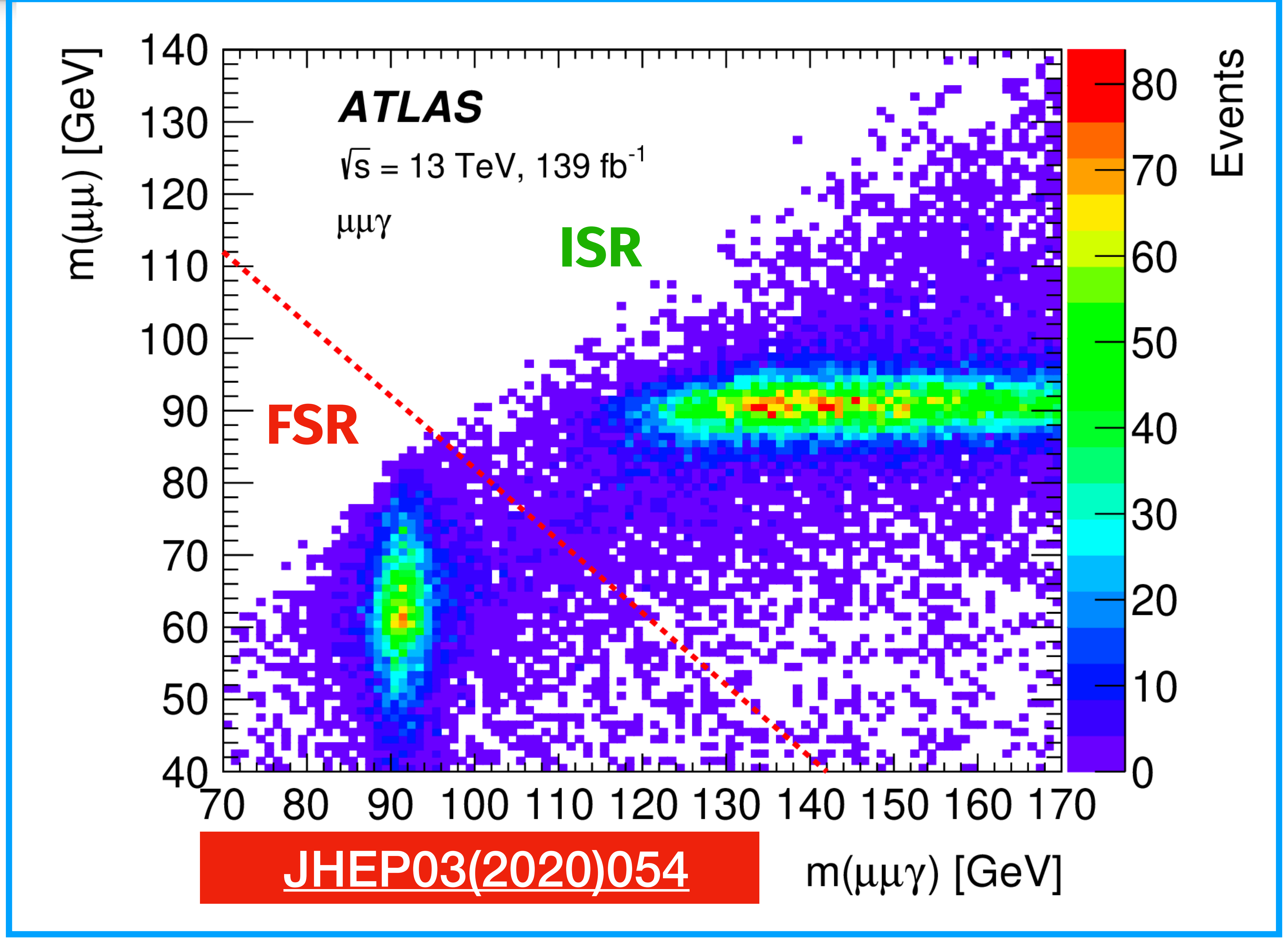

- First measurement concerning jet activities
  - Additional jets could come from gluon splitting, etc
  - Jet inclusive measurement: JHEP03(2020)054
  - Sensitive to QCD effects
- Interested in ISR events (photon radiated from initial quarks)
  - FSR events simply Drell-Yan process

- Dedicated cut on $m_{ll} + m_{ll\gamma}$ to suppress FSR
- Require $m_{ll} > 40\ GeV$ to suppress Drell-Yan
- Data-Driven estimate for jet-fake-photon and pile-up photon

Zγ+Jets Differential

JHEP 07 (2023) 072

- Fiducial differential XS measured for:
  - 1D kinematic observables of lepton, jet and photon
  - Pseudo-2D jet observables sensitive to fixed order perturbative QCD (pQCD) calculations
  - 2D variables sensitive to Z boson polarization in Collins-Soper frame
- Overall good agreement with theory predictions
  - NLO QCD improves both inclusive XS as well as the modeling of variables
  - $Measured : 533.7 \pm 15.5\ (total)\ fb\ ;\ sherpa\ LO :\ 438.9 \pm 0.6\ (stat)\ fb$
  - $Sherpa\ NLO : 479.5 \pm 0.3\ (stat)\ ; MiNNLO_{PS} : 493.0 \pm 3.0\ (stat)$

N_{jets}	0	1	2	> 2
Source	Uncertainty [%]			
Electrons	1.0	0.9	0.8	0.8
Muons	0.3	0.3	0.3	0.4
Jets	1.7	1.7	4.5	8.8
Photons	1.4	1.3	1.3	1.2
Pile-up	2.1	0.8	0.2	0.3
Background	1.8	1.8	3.0	4.4
MC statistical	0.1	0.2	0.3	0.4
Data statistical	0.8	1.5	1.8	1.9
Luminosity	1.7	1.7	1.7	1.7
Theory	0.6	0.2	1.4	1.0
Total	4.2	3.8	6.3	10.3

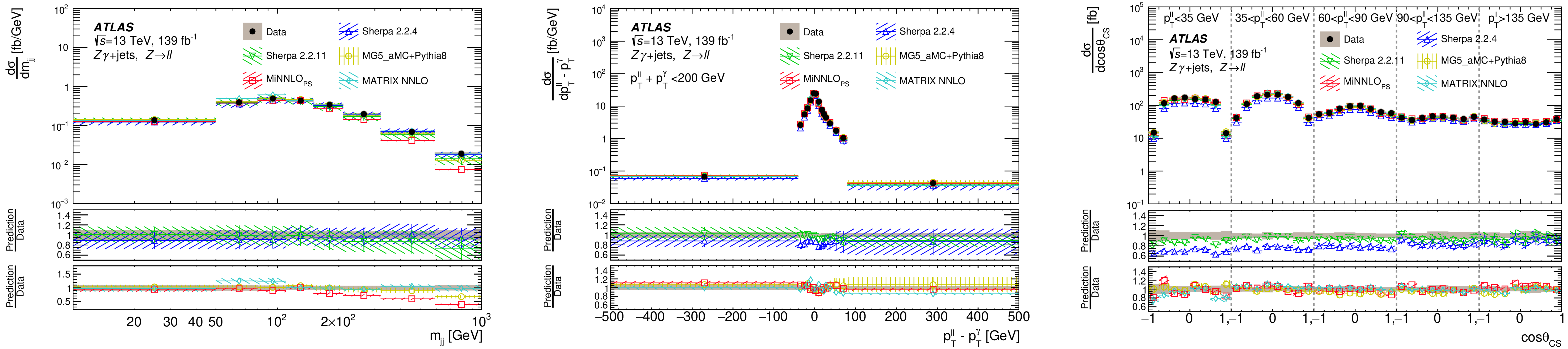

ZZ->4l Angular Analysis

ATLAS-CONF-2023-038

Evidence for $Z_L Z_L$ polarization state

- Dedicated BDT template built for 3 polarization states
- Reweighted to latest $M_O C_A NLO$ program calculation
  - NLO QCD and EW correction
  - Loop-induced $gg \to ZZ$ correction

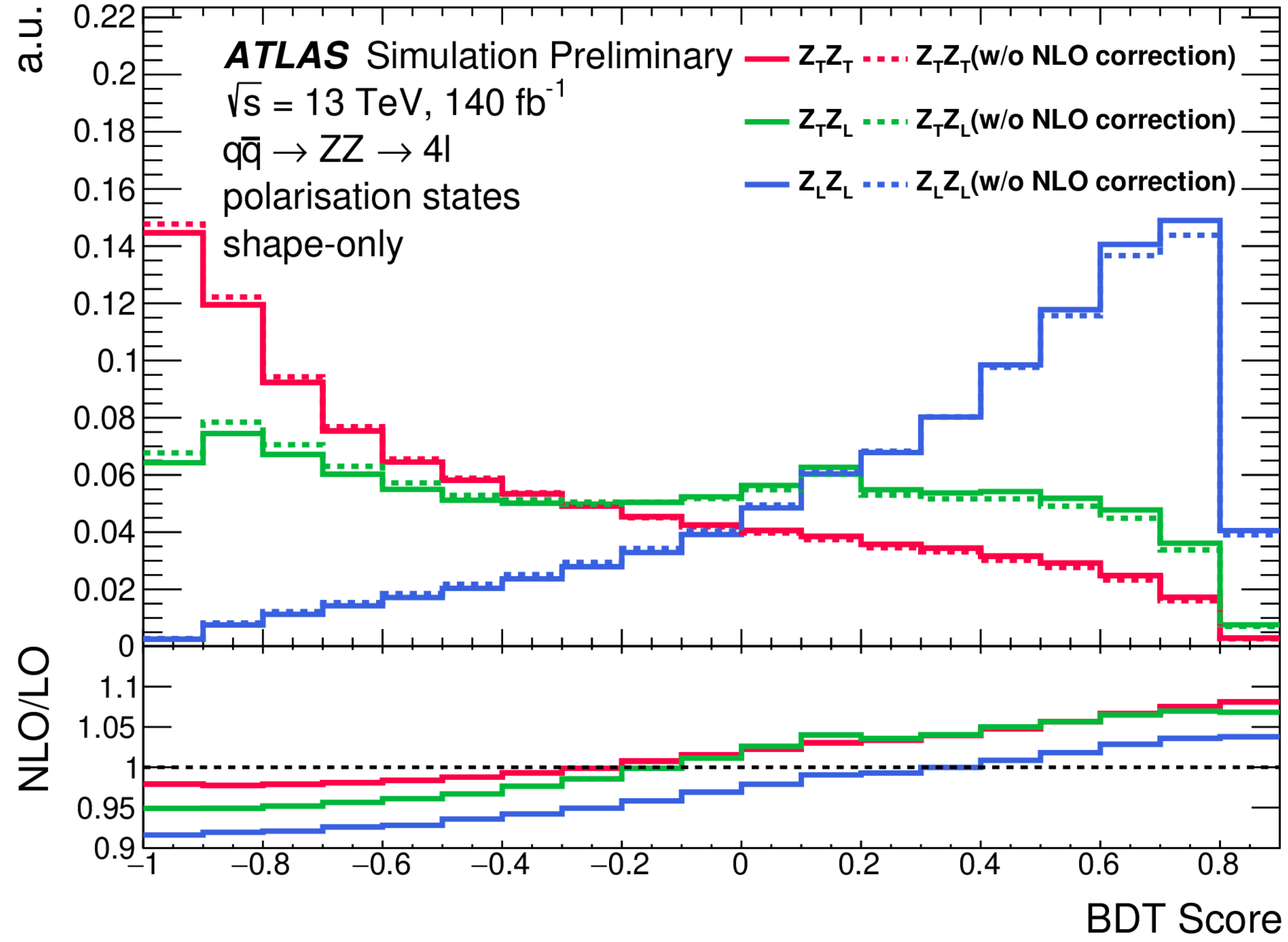

ZZ CP study

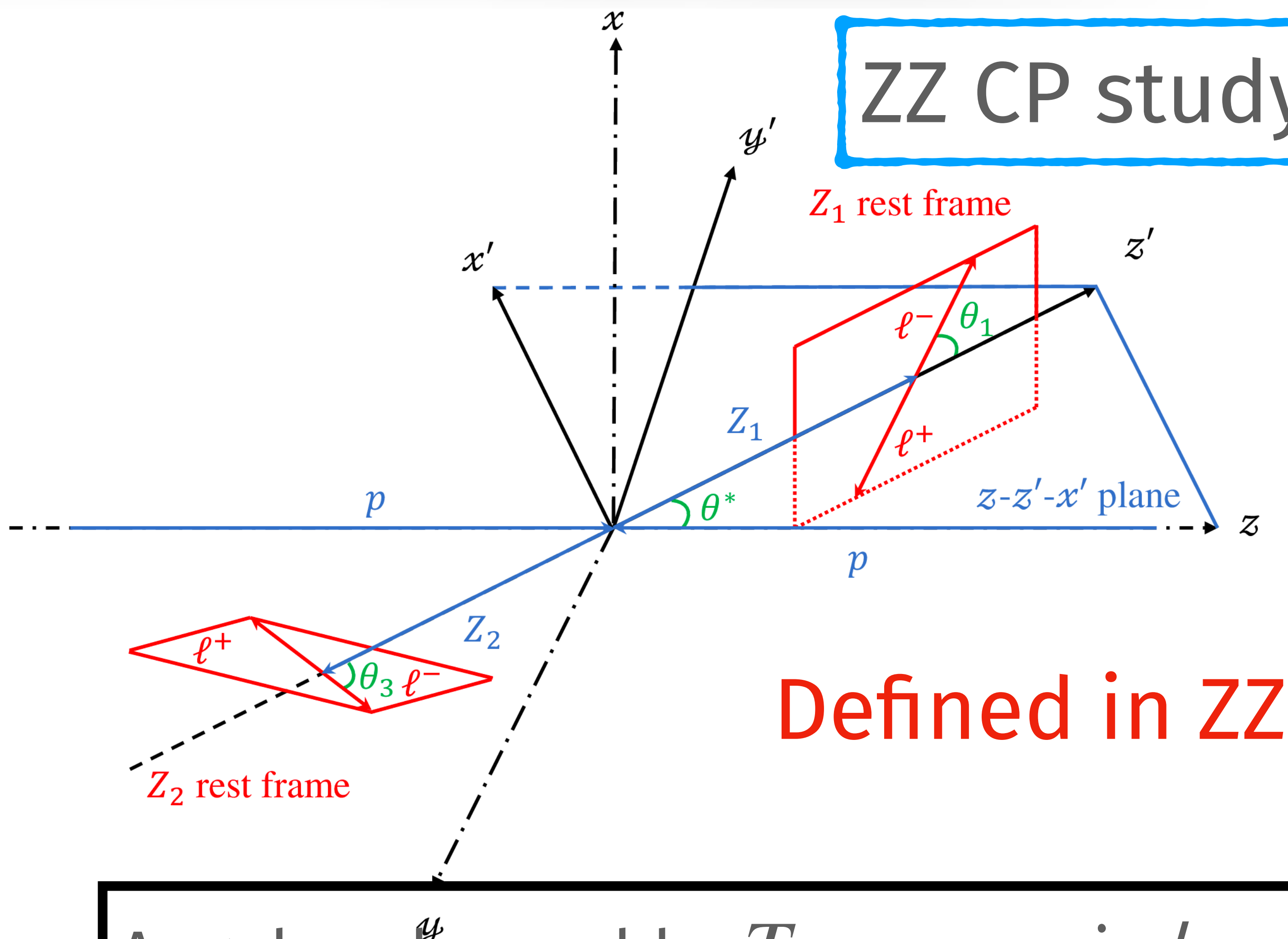

Defined in ZZ rest frame

Angular observable: $T_{yz,1(3)} = sin\phi_{1(3)} \times cos\theta_{1(3)}$

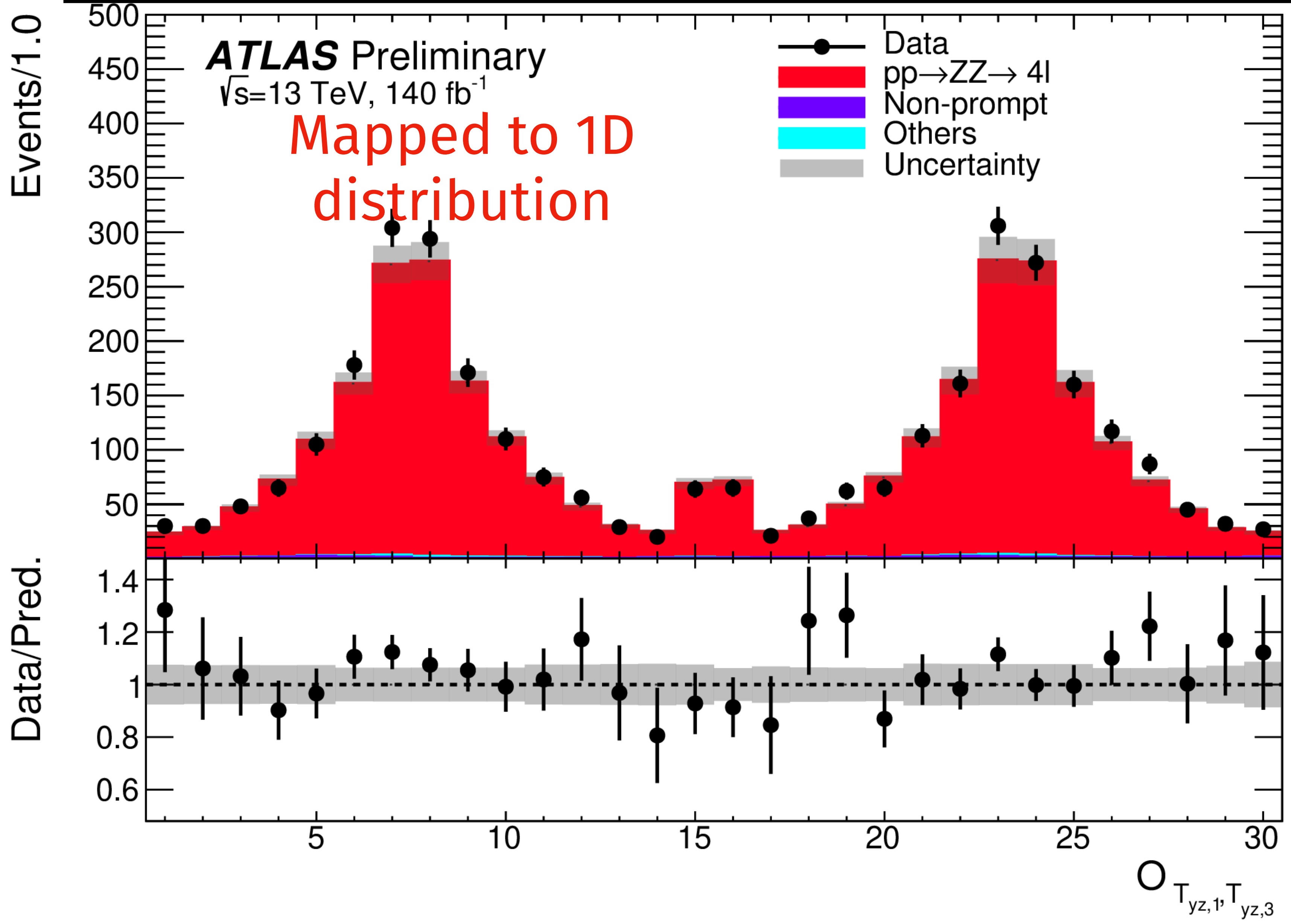

ZZ->4l Angular Analysis

ATLAS-CONF-2023-038

- Binned profile likelihood fit sum of reweighed BDT templates to data
- Significance of $Z_L Z_L$: 4.3σ *obs* $(3.8\sigma$ *exp*$)$
- Fiducial XS: $\sigma^{obs}_{Z_L Z_L} = 2.44 \pm 0.59\ fb$

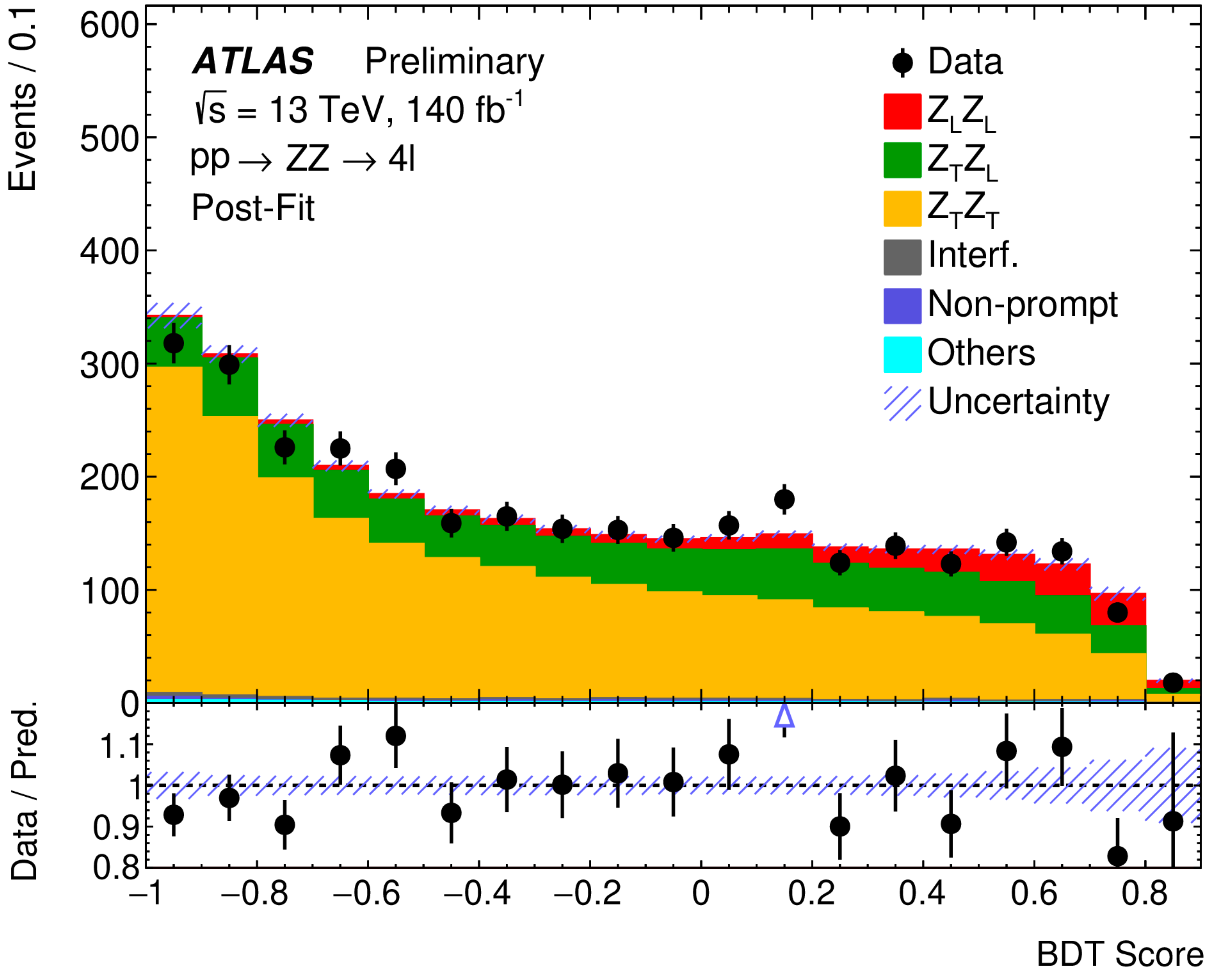

Unfolded $O_{T_{yz,1},T_{yz,3}}$ to data

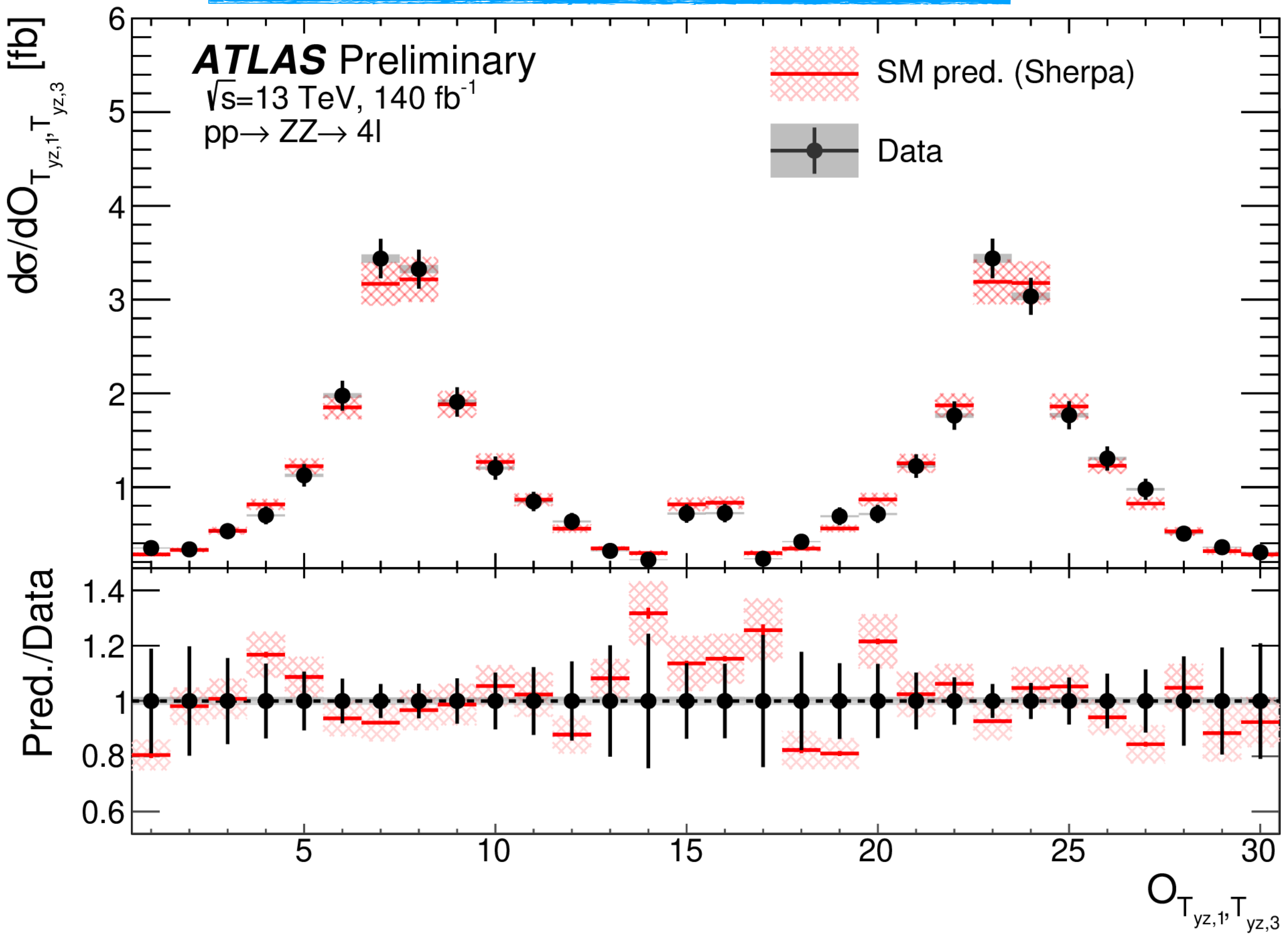

aNTGC parameter	Interference only Expected	Interference only Observed	Full Expected	Full Observed
f_Z^4	$[-0.16, 0.16]$	$[-0.12, 0.20]$	$[-0.013, 0.012]$	$[-0.012, 0.012]$
f_γ^4	$[-0.30, 0.30]$	$[-0.34, 0.28]$	$[-0.015, 0.015]$	$[-0.015, 0.015]$

Reinterpreted to CP-odd aNTGC Model

ZZ->4l Run 3

ATLAS-CONF-2023-062

- First ZZ measurement in Run 3
  - Using data collected in 2022 ~ 29 fb^{-1}
- Fiducial and differential XS measurements
  - Fiducial XS extrapolated to full phase space total XS
  - Differential XS measured for m_{4l} and p_{4l}^{T}

NEW

Both Z boson on-shell, agree with predictions within uncertainty

	Measurement	MC prediction	MATRIX prediction
Fiducial	$36.7 \pm 1.6(\text{stat}) \pm 1.5(\text{syst}) \pm 0.8(\text{lumi})$ fb	$36.8\ ^{+4.3}_{-3.5}$ fb	36.5 ± 0.6 fb
Total	$16.9 \pm 0.7(\text{stat}) \pm 0.7(\text{syst}) \pm 0.4(\text{lumi})$ pb	$17.0\ ^{+1.9}_{-1.4}$ pb	16.7 ± 0.4 pb

First point at 13.6 TeV!

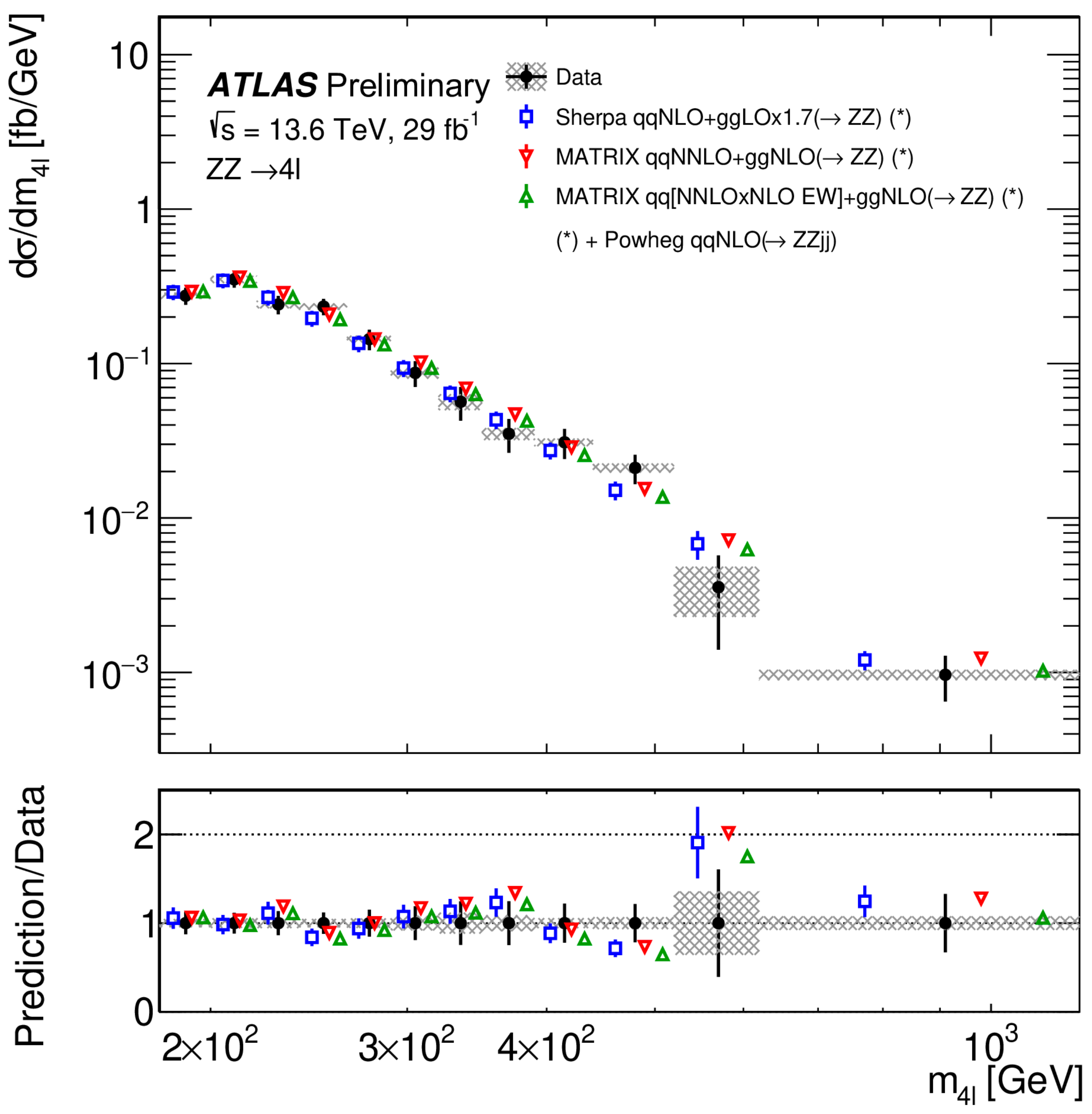

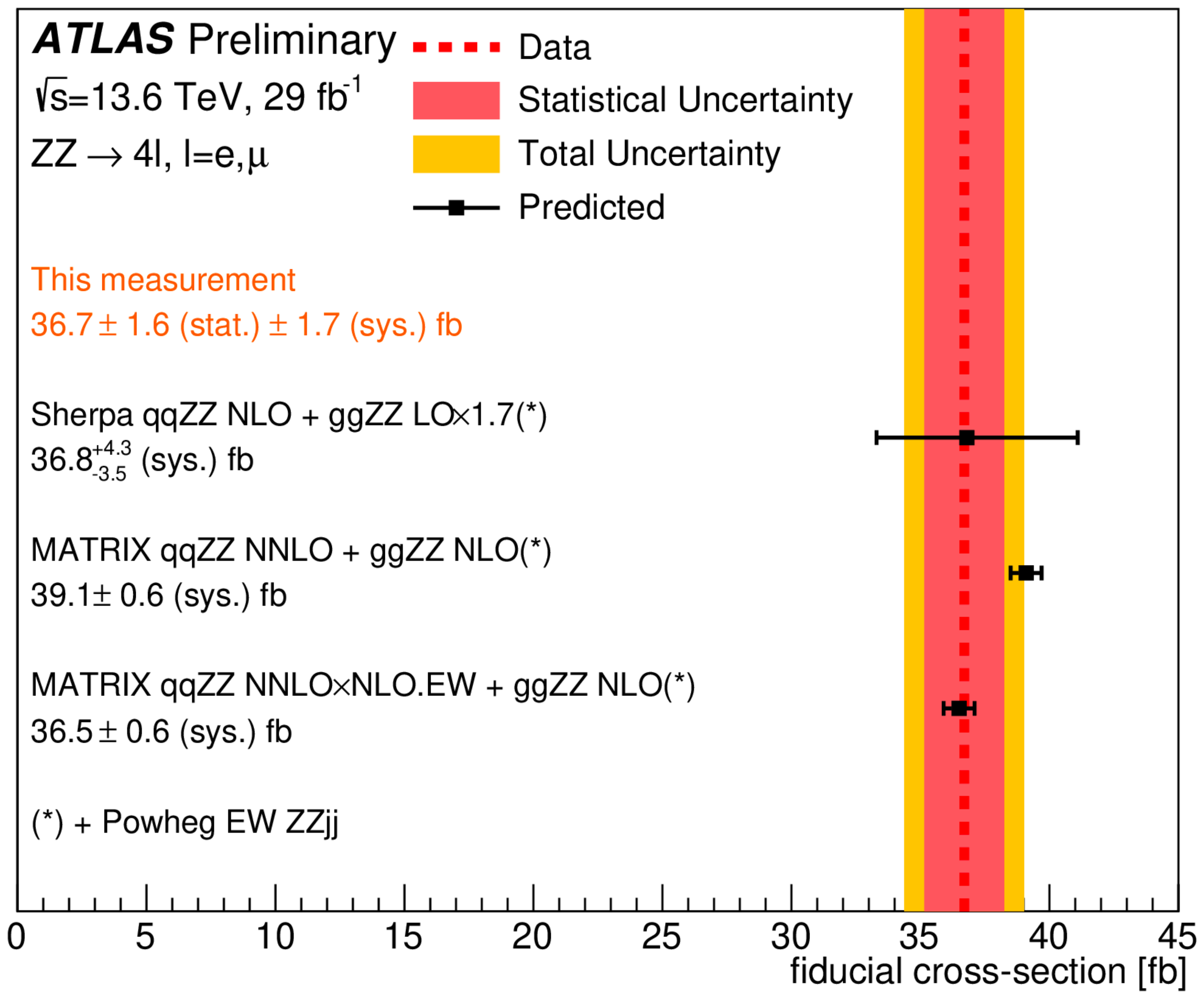

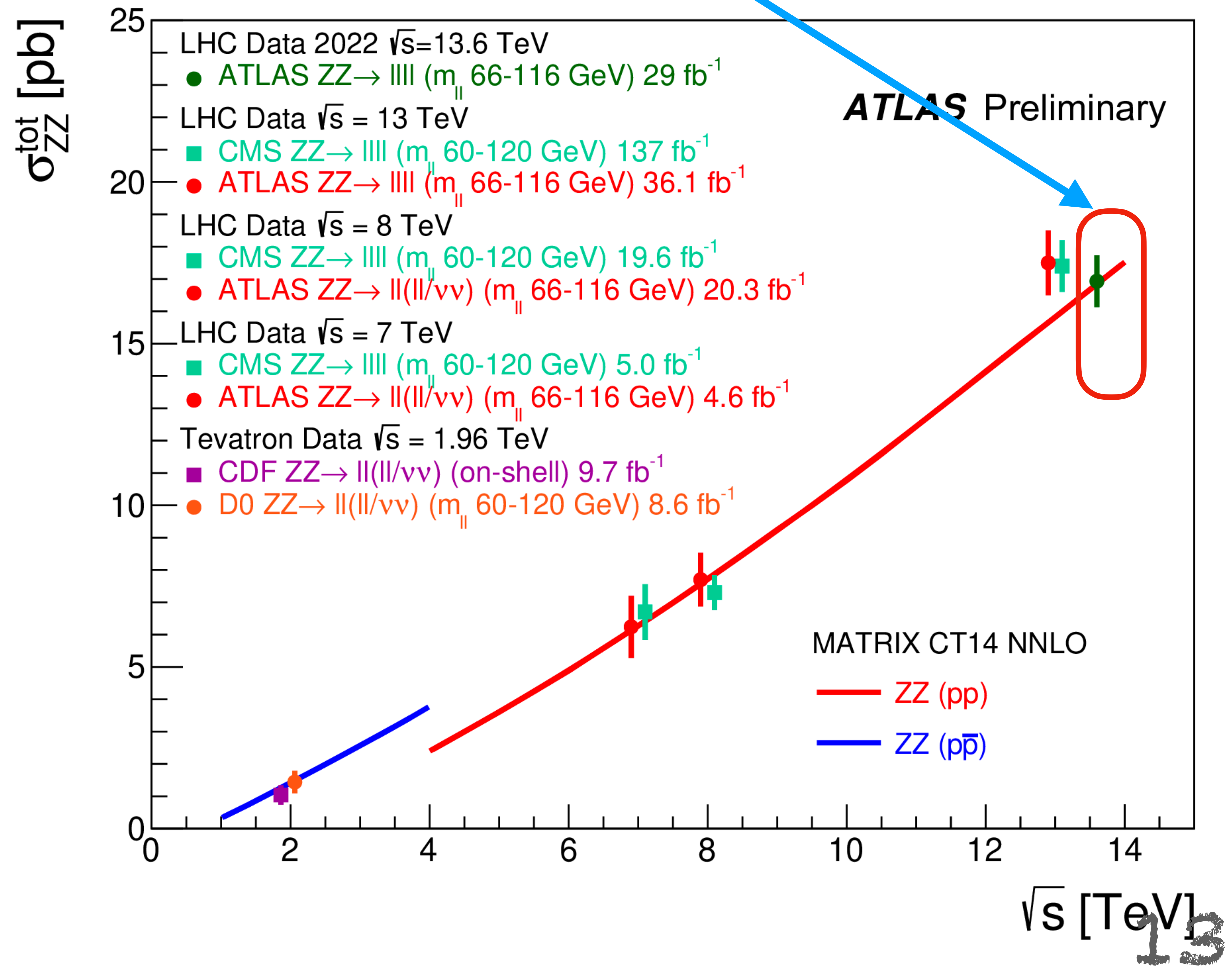

ZZ+Jets Differential

CMS-PAS-SMP-22-001

- Measurement of ZZ production
  - LO t-channel: s-channel forbidden at SM
  - Gluon-gluon fusion via box diagram -> 10% contribution
- On-shell Z boson, leptonic decay
  - Require $60\ GeV < m_{Z_1,Z_2} < 120\ GeV$
  - $ZZ \to 2l2l'$
- Background extremely suppress by 4-lepton requirement
- Differential XS measured as functions of:
  - Number of jets
  - Kinematic variables of jets
  - m_{4l} as a function of jet multiplicity

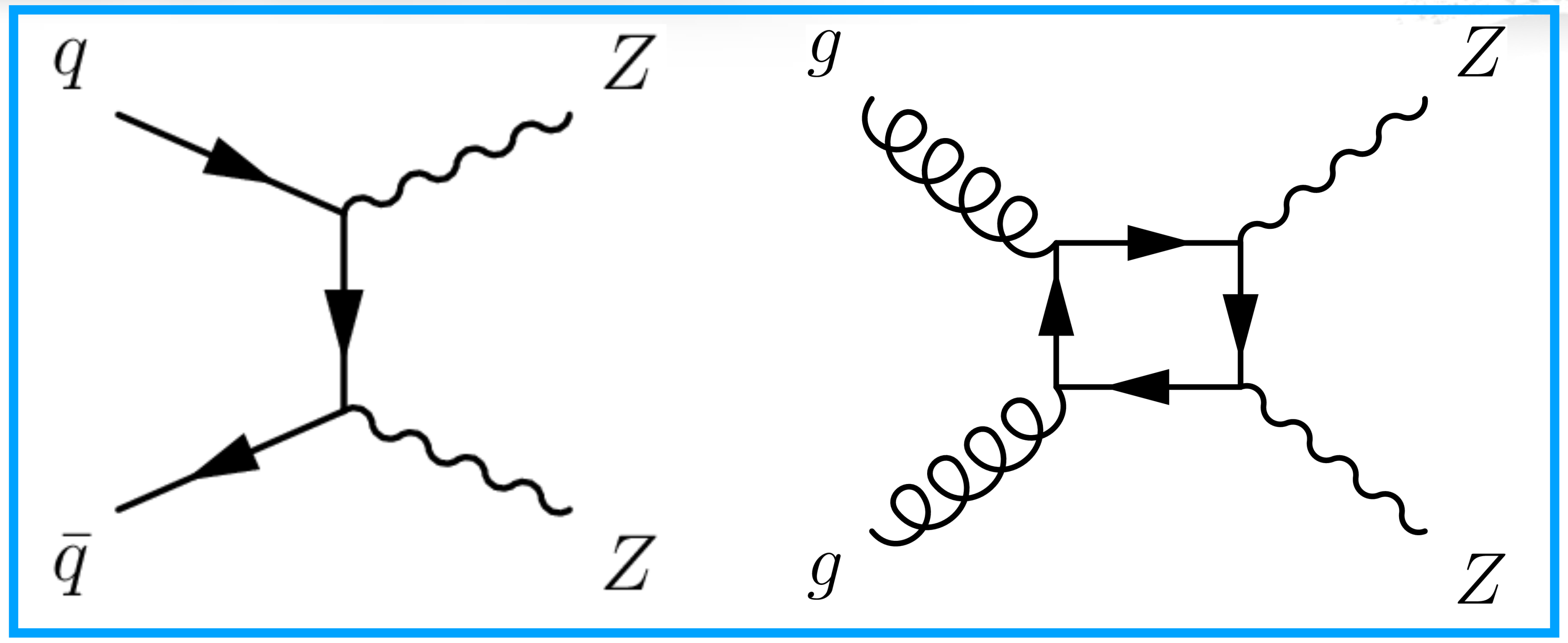

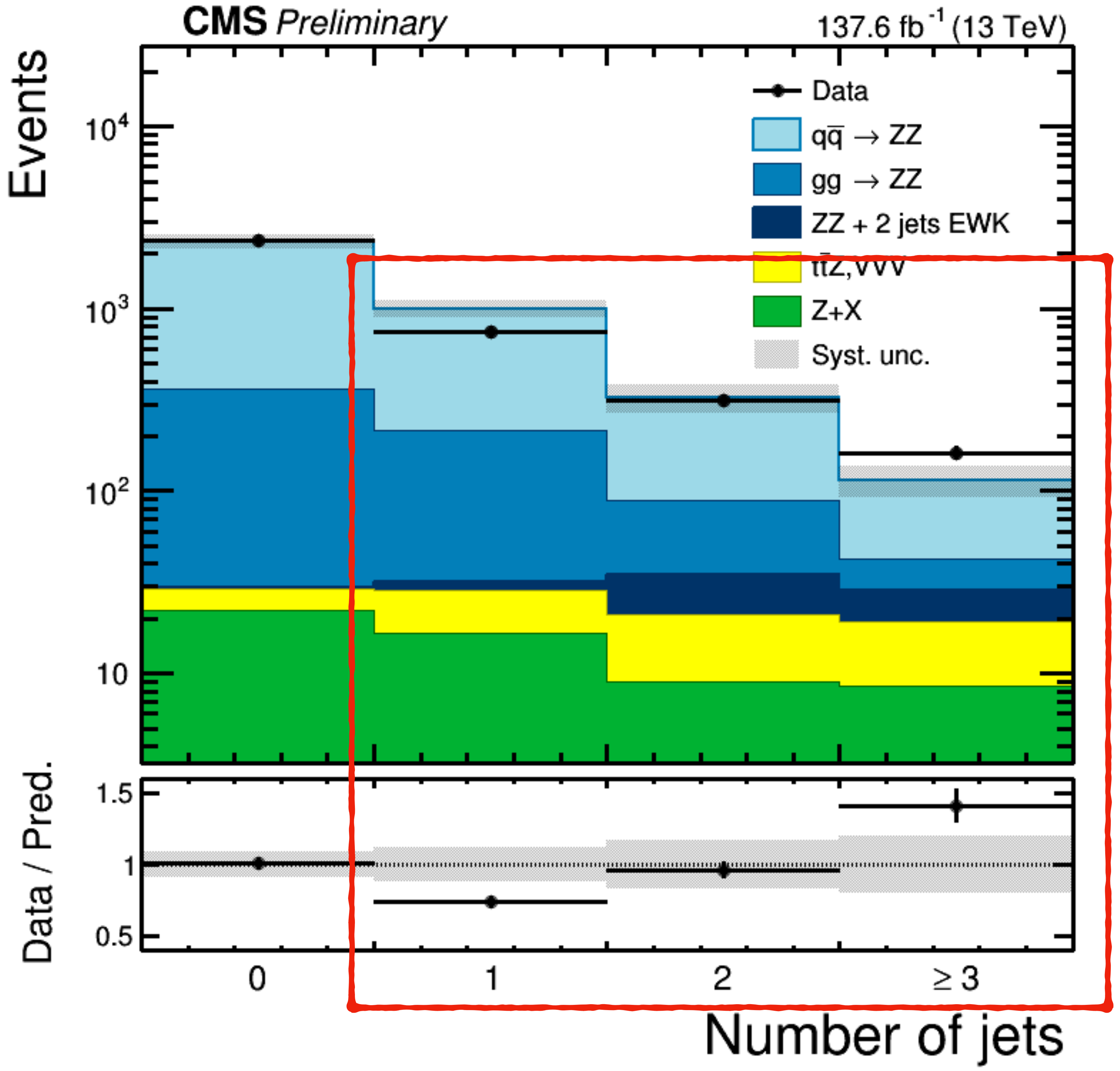

ZZ+Jets Differential

CMS-PAS-SMP-22-001

- Differential XS normalized to the fiducial XS
- Theory predictions over-estimate data
- Large discrepancy at high jet pt region
- Main systematic uncertainties: jet, QCD scales

Systematic source	$m_{4\ell}$ with all jets	0 jet	1 jet	2 jets	3 and more jets
Trigger	-	-	-	-	-
Electron Efficiency	0.42 %	0.38 %	0.66 %	0.36 %	0.26 %
Muon Efficiency	0.05 %	0.06 %	0.07 %	0.09 %	0.08 %
Jet energy resolution	0.0	0.07 %	1.72 %	1.65 %	0.8 %
JES correction	0.0	0.17 %	1.77 %	1.95 %	0.97 %
Reducible background	0.18 %	0.18 %	0.32 %	0.33 %	0.96 %
Pileup	0.02 %	0.05 %	0.11 %	0.13 %	0.35 %
Luminosity	0.01 %	0.01 %	0.02 %	0.02 %	0.05 %
Monte Carlo choice	0.35 %	0.65 %	0.94 %	0.48 %	0.35 %
gg cross section	0.02 %	0.03 %	0.09 %	0.06 %	0.09 %
QCD Scales	0.15 %	0.16 %	0.58 %	0.54 %	0.62 %
PDF	0.05 %	0.05 %	0.15 %	0.15 %	0.21 %
α_S	0.02 %	0.01 %	0.05 %	0.03 %	0.02 %

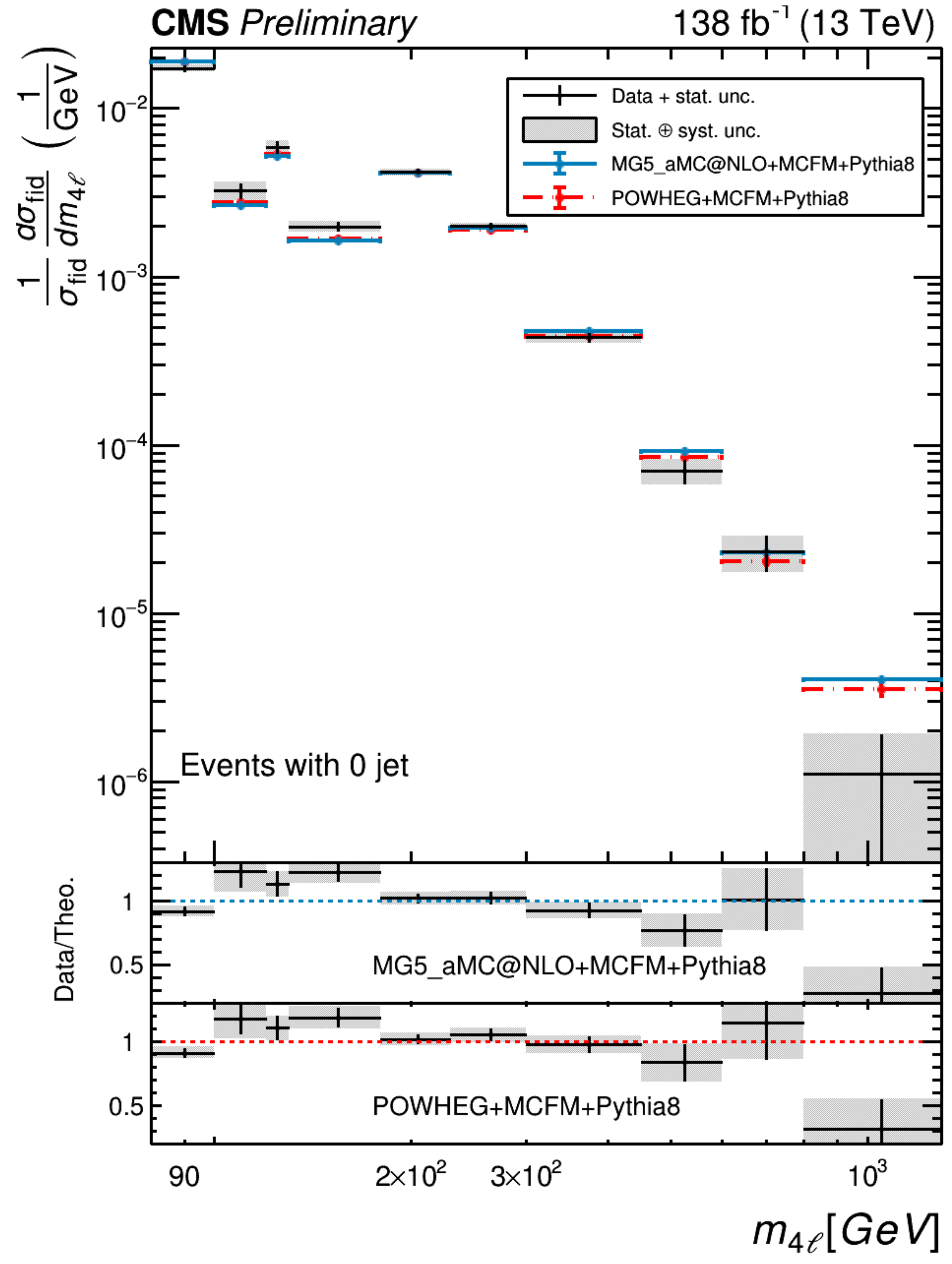

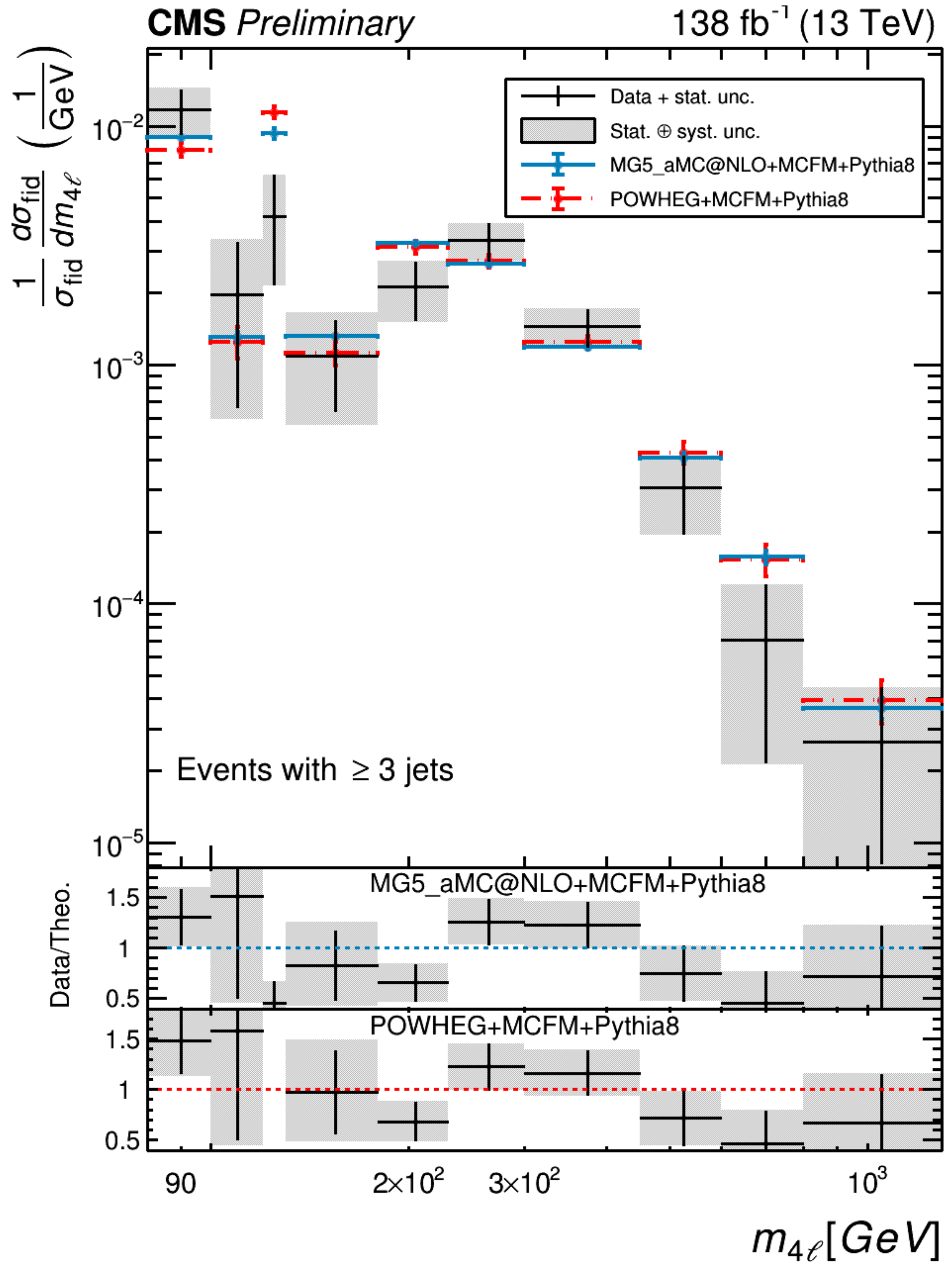

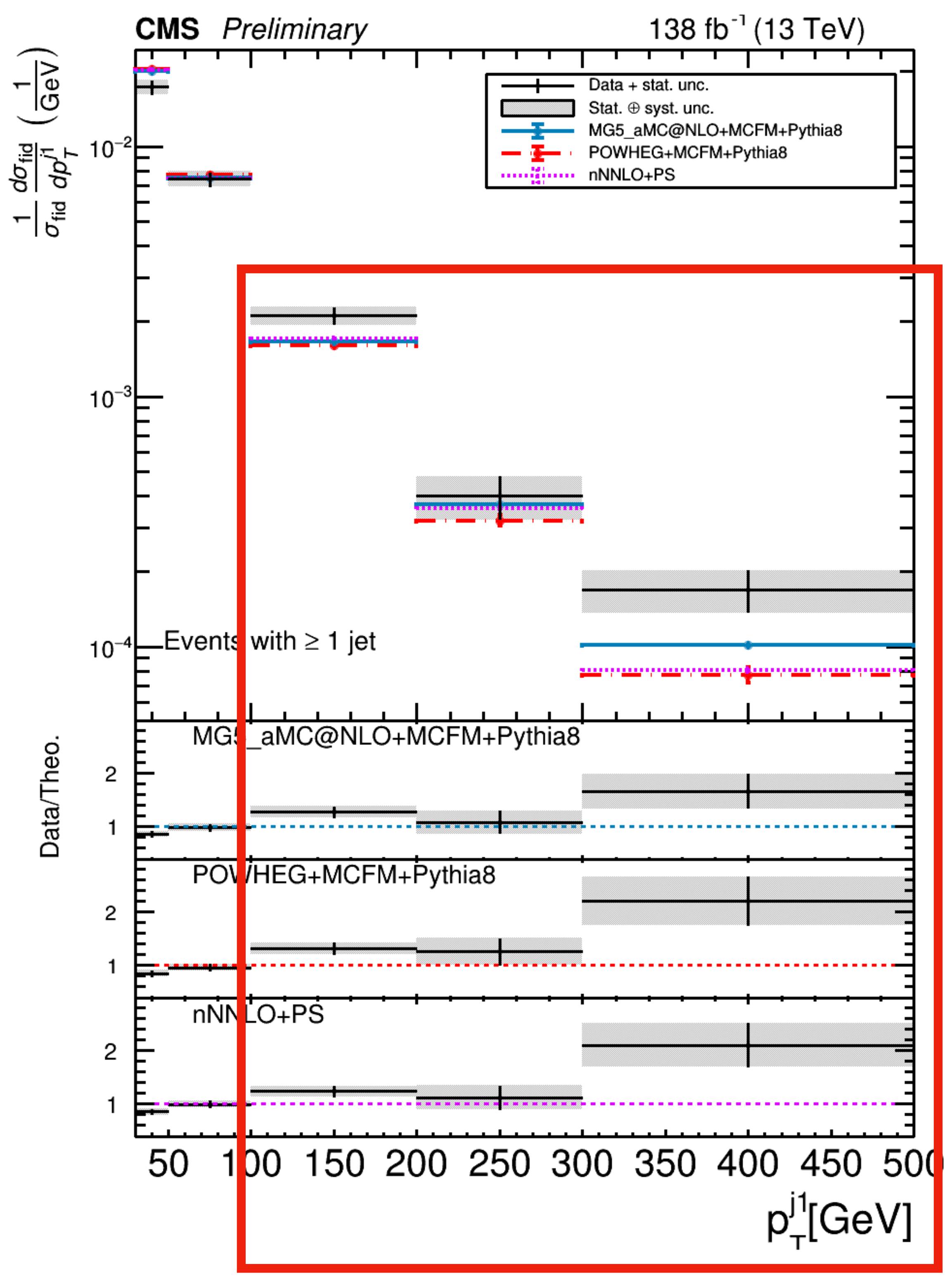

Disagreement at high jet pt region

Search for γγ->VV

CMS-SMP-21-014

- Search for exclusive high-mass $\gamma\gamma \to W^+W^-$, $\gamma\gamma \to ZZ$
- Intact forward proton tagged by Precision Proton Spectrometer (PPS)
  - Center-of-mass energy of di-photon collision determined event-by-event
  - Events recorded by both CMS and TOTEM -> 100 fb^{-1}
- Hadronically decaying W or Z bosons
  - Boosted to two fat-jets
  - $m_{jj} > 1126\ GeV$
  - $m_{j1} + m_{j2} = 166.6\ GeV$ to separate WW/ZZ events
- SR defined based on jet-proton matching

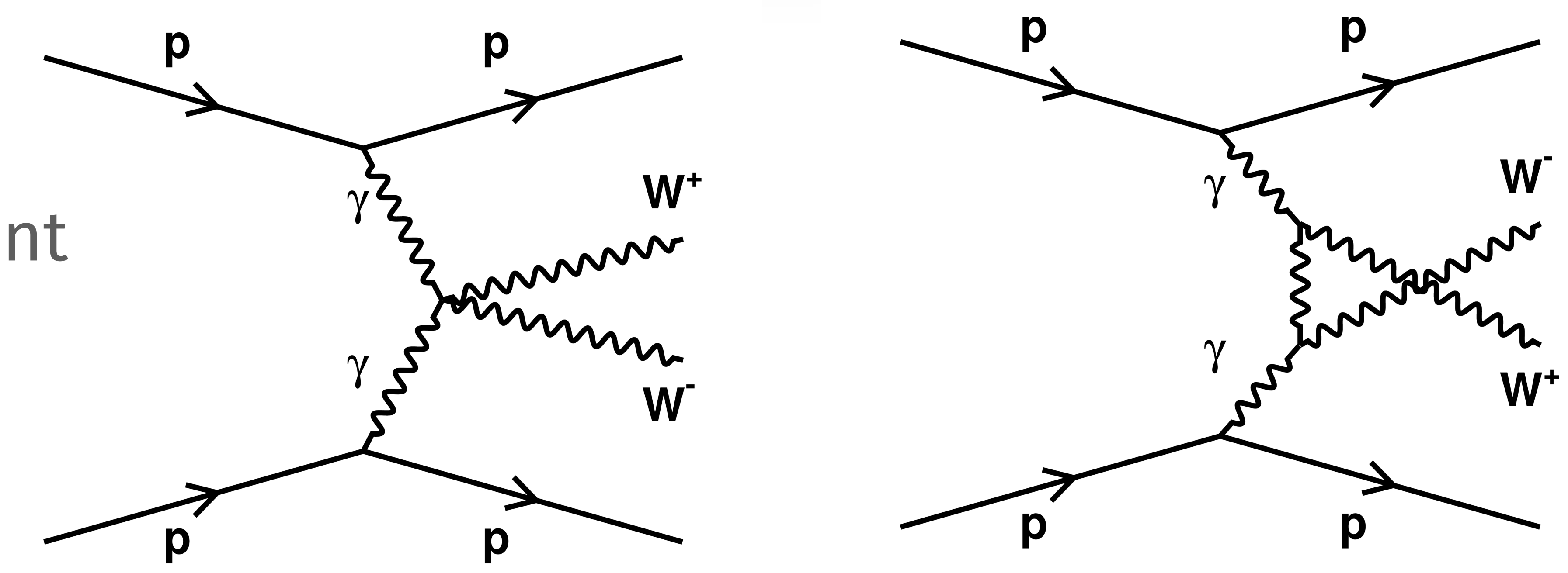

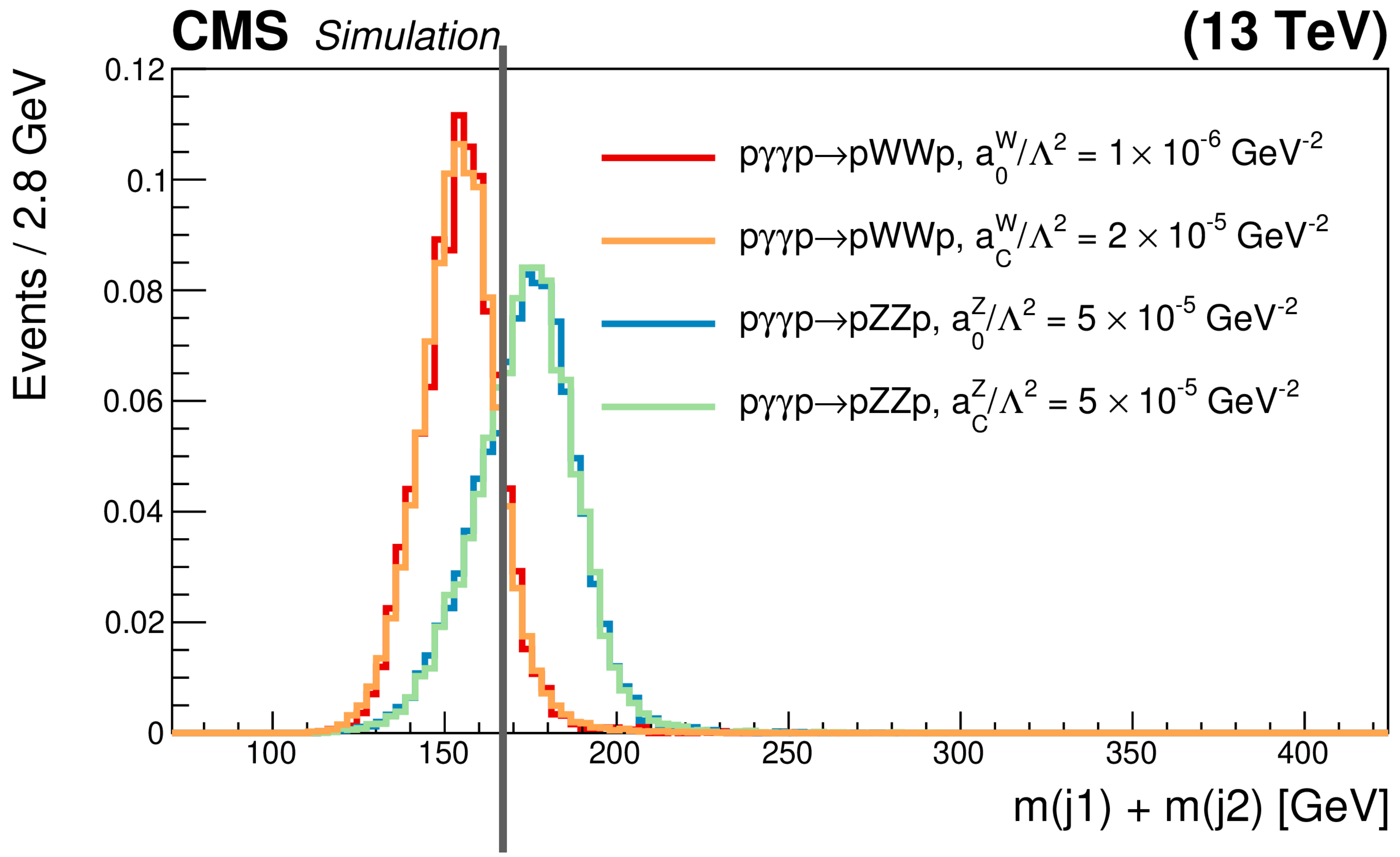

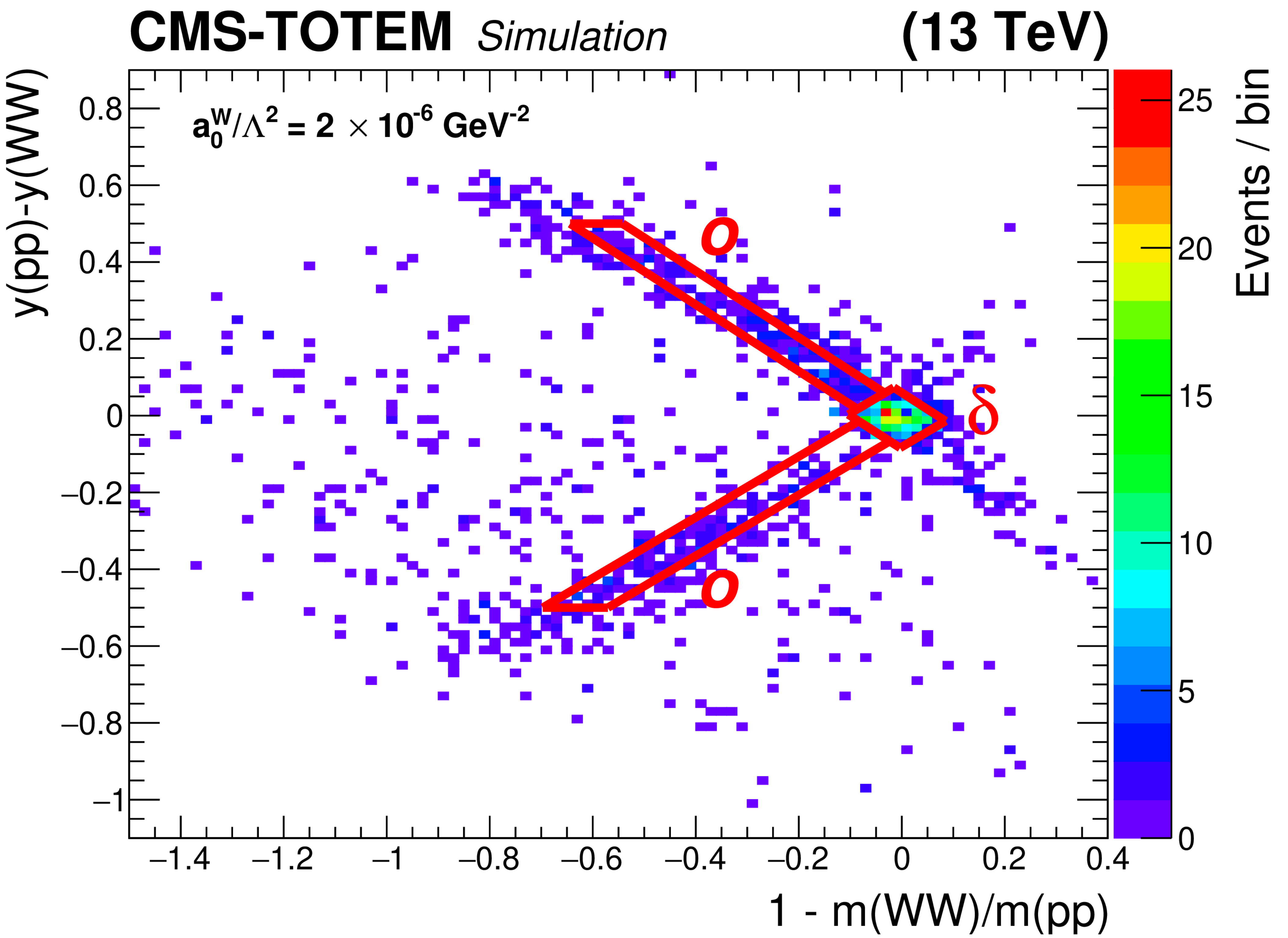

Search for γγ->VV

CMS-SMP-21-014

- Signal extracted by binned maximum-likelihood fit in 12 bins
- No excess of AQGC signal observed
- Upper limit set on dimension-6 AQGC operators
  - 15% improvement comparing to previous result
  - Also translation to linear dimension-8 AQGC operators
- Upper limit on AQCG fiducial cross section:
  - $\sigma_{fid}(pp \rightarrow pWWp) < 67\ (53^{+34}_{-19})\ fb$
  - $\sigma_{fid}(pp \rightarrow pZZp) < 43\ (62^{+33}_{-20})\ fb$

Coupling	Observed (expected) 95% CL upper limit No clipping	Observed (expected) 95% CL upper limit Clipping at 1.4 TeV
$\lvert a_0^W/\Lambda^2 \rvert$	$4.3\ (3.9) \times 10^{-6}\,\mathrm{GeV}^{-2}$	$5.2\ (5.1) \times 10^{-6}\,\mathrm{GeV}^{-2}$
$\lvert a_C^W/\Lambda^2 \rvert$	$1.6\ (1.4) \times 10^{-5}\,\mathrm{GeV}^{-2}$	$2.0\ (2.0) \times 10^{-5}\,\mathrm{GeV}^{-2}$
$\lvert a_0^Z/\Lambda^2 \rvert$	$0.9\ (1.0) \times 10^{-5}\,\mathrm{GeV}^{-2}$	—
$\lvert a_C^Z/\Lambda^2 \rvert$	$4.0\ (4.5) \times 10^{-5}\,\mathrm{GeV}^{-2}$	—

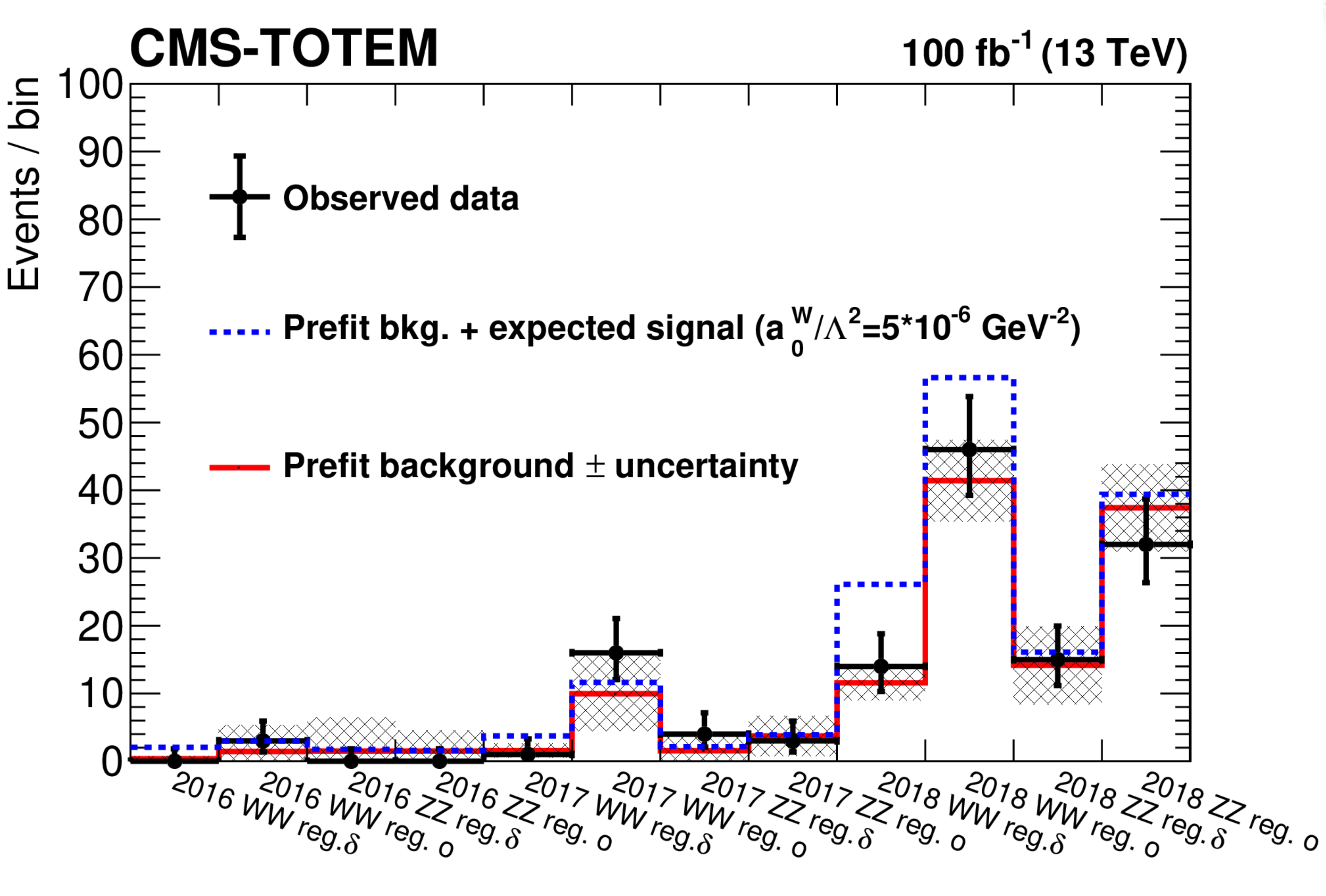

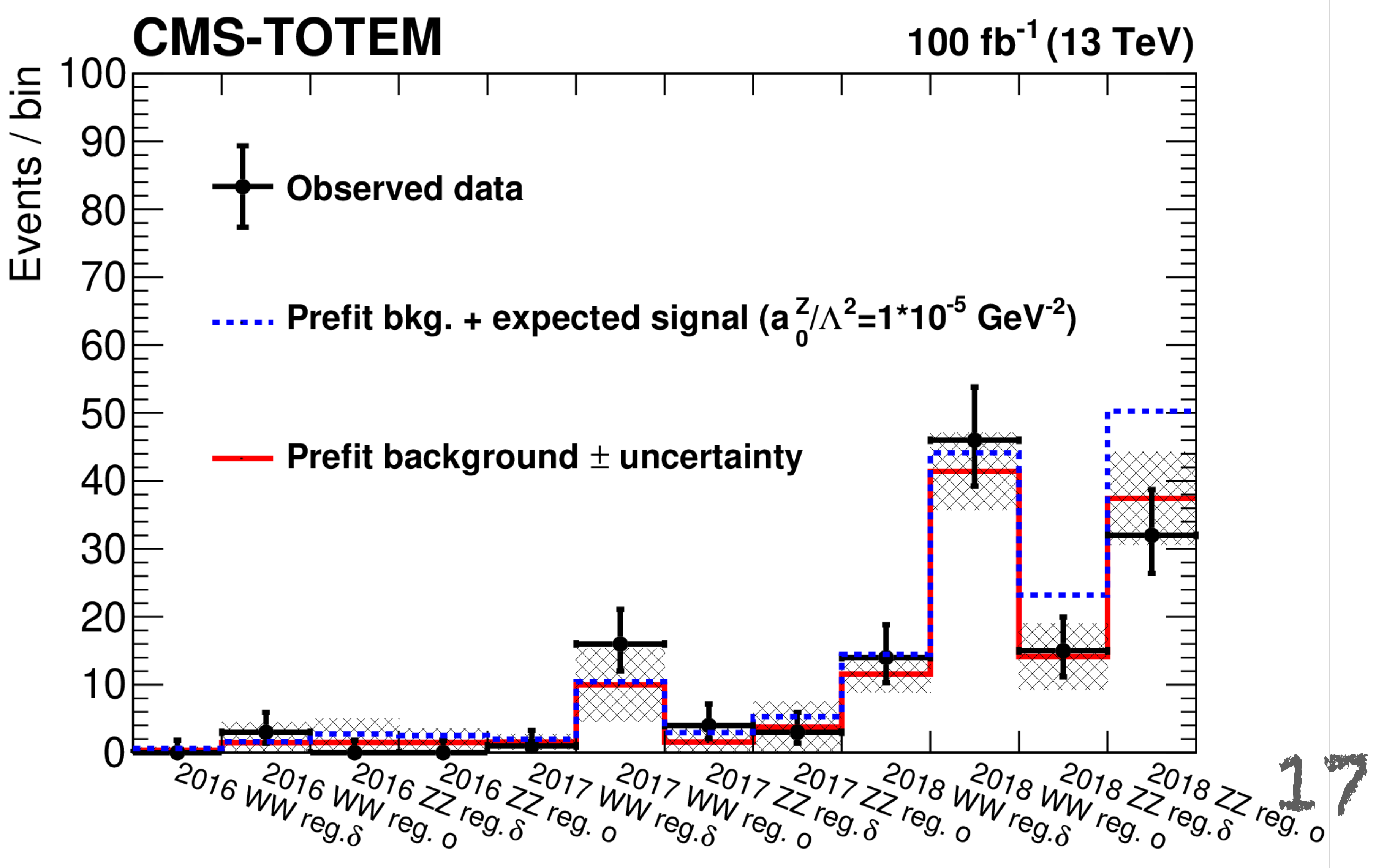

Summary

- Recent Diboson production cross section measurements and polarization measurements from ATLAS and CMS collaborations presented
  - Several new techniques developed to improve precision and search for rare processes
    - Machine Learning plays an more and more important role in the SM analysis!
    - Data-driven methods to estimate backgrounds not well modeled by simulation
  - Many new observations and evidences of longitudinal polarized vector boson
    - $W_L Z_L$ state has been observed
    - Evidence of $Z_L Z_L$ state, very close to observation
  - So far good agreement with state-of-art calculations, no evidence of anomalous couplings
- Stay tuned for new Run 3 results!

Backup Material

W+W- Jet Inclusive

ATLAS-CONF-2023-012

The number of $t\bar{t}$ events in the two control regions and the signal region, after subtracting non-$t\bar{t}$ backgrounds, is parametrized using three parameters. The first is the number of $t\bar{t}$ events without requirements on the b-jet multiplicity, $N^{t\bar{t}}_{\geq 0b}$. The second is the efficiency of identifying and selecting a b-jet in a $t\bar{t}$ event, ε_b, accounting for the efficiency of the b-tagging algorithm as well as the acceptance of b-jets. The third is the b-jet correlation factor C_b, which takes into account that the probability of identifying both b-jets in a $t\bar{t}$ events is not exactly ε_b^2 but $C_b\varepsilon_b^2$, due to correlation effects that depend on the interplay of event selection and $t\bar{t}$ kinematics as well as the presence of additional light jets and b-jets. The number of $t\bar{t}$ events with exactly i b-tagged jets, $N^{t\bar{t}}_{ib}$, is given by

$$N^{t\bar{t}}_{2b} = N^{t\bar{t}}_{\geq 0b} \cdot C_b\varepsilon_b^2 \,, \quad (1)$$

$$N^{t\bar{t}}_{1b} = N^{t\bar{t}}_{\geq 0b} \cdot \left(2\varepsilon_b - C_b\varepsilon_b^2\right) \,, \quad (2)$$

$$N^{t\bar{t}}_{0b} = N^{t\bar{t}}_{\geq 0b} \cdot \left(1 - 2\varepsilon_b + C_b\varepsilon_b^2\right) \,. \quad (3)$$

Using these equations, the number of $t\bar{t}$ events in the signal region can be expressed as

$$N^{t\bar{t}}_{0b} = \frac{C_b}{4}\frac{\left(N^{t\bar{t}}_{1b} + 2N^{t\bar{t}}_{2b}\right)^2}{N^{t\bar{t}}_{2b}} - N^{t\bar{t}}_{1b} - N^{t\bar{t}}_{2b} \,, \quad (4)$$

Data-driven estimate method for top backgrounds

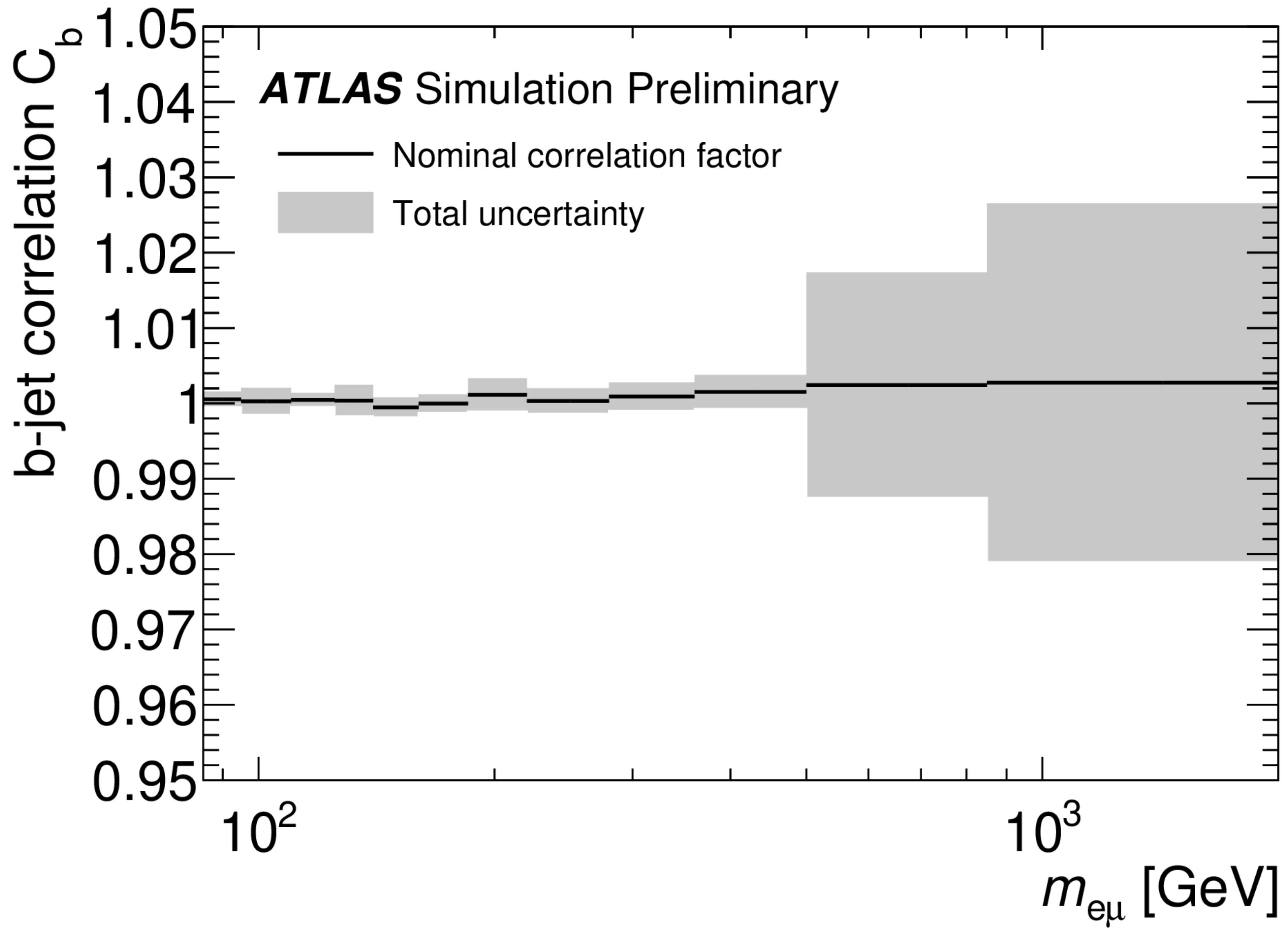

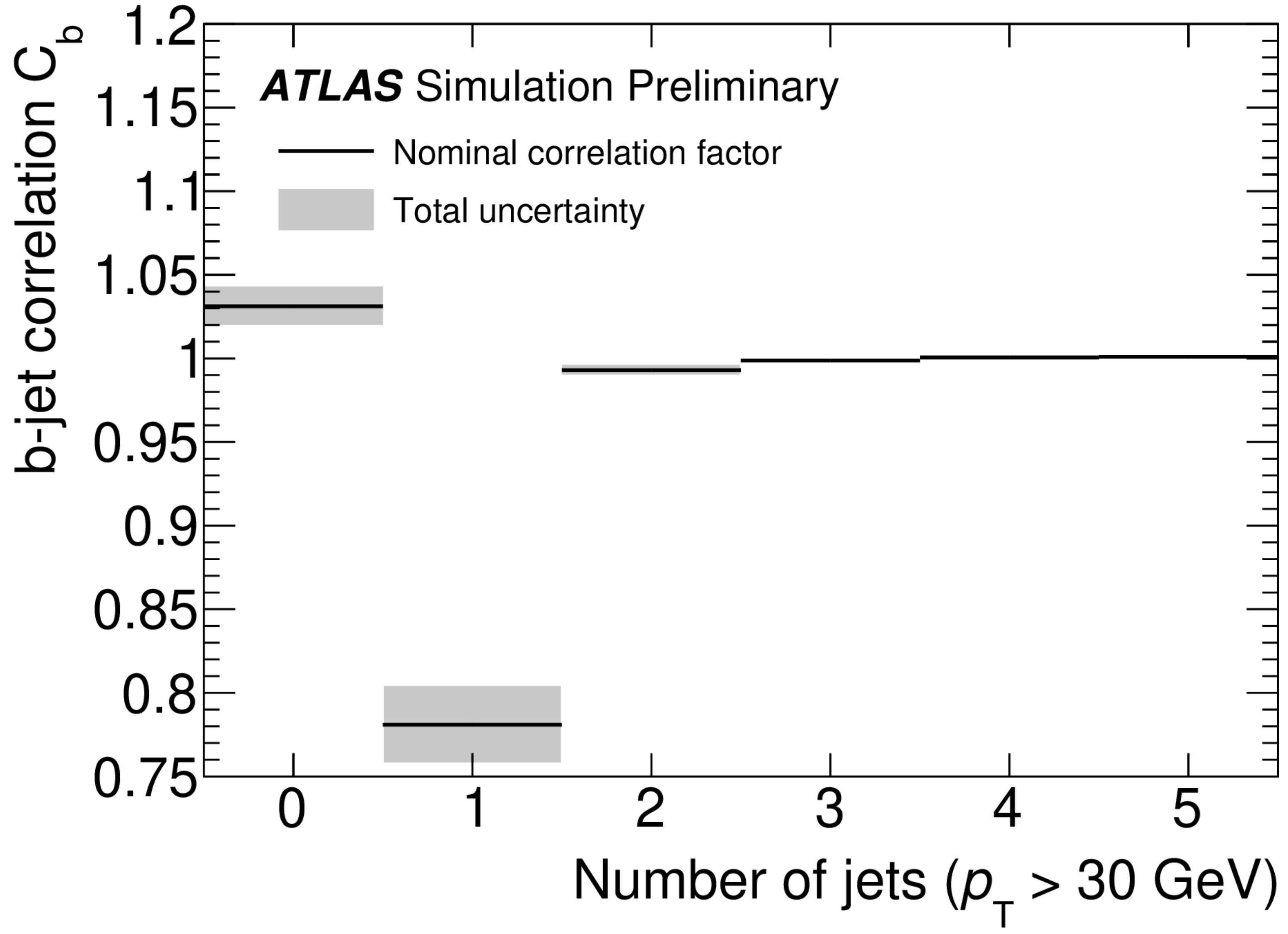

W+W- Jet Inclusive

ATLAS-CONF-2023-012

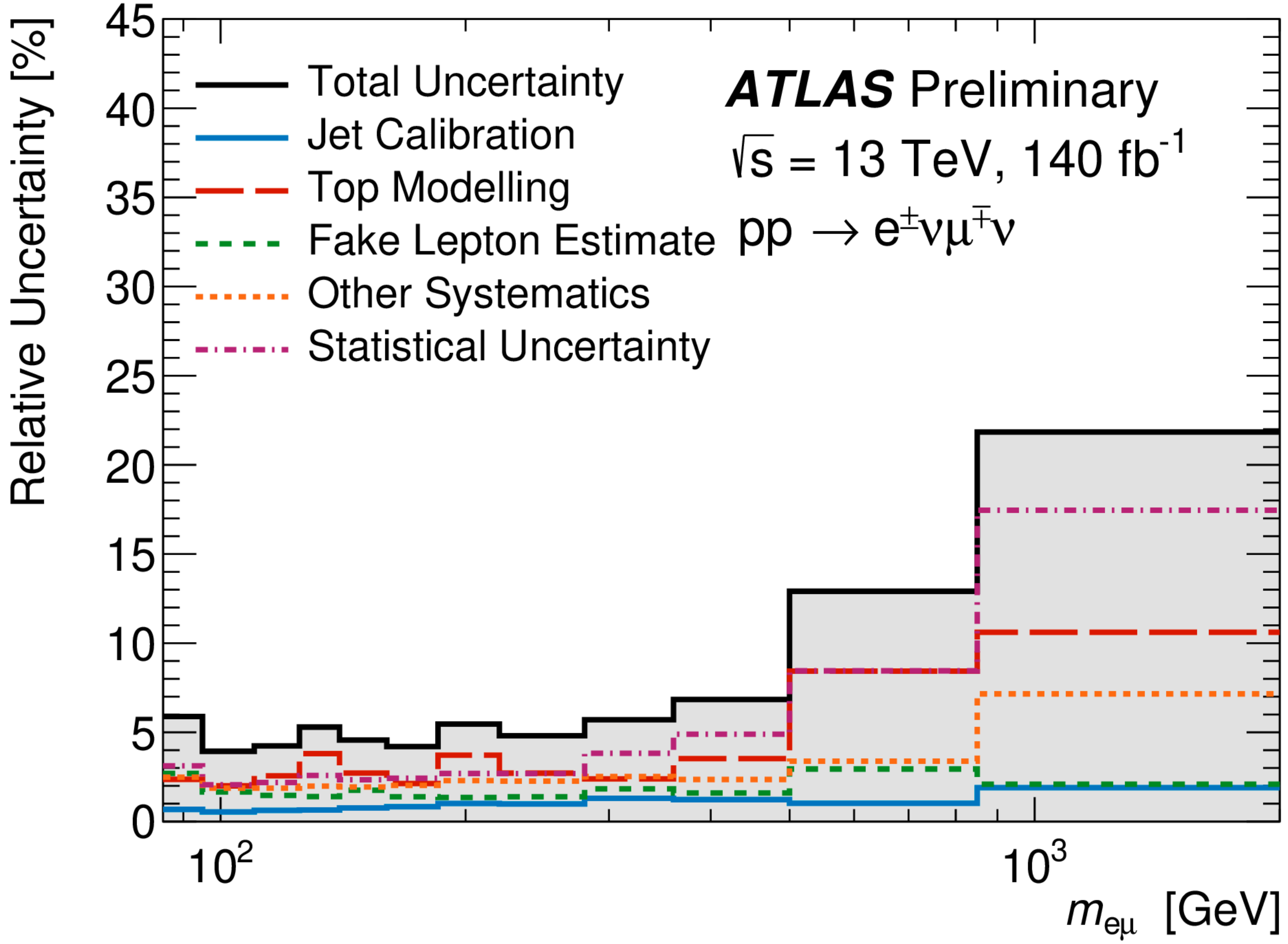

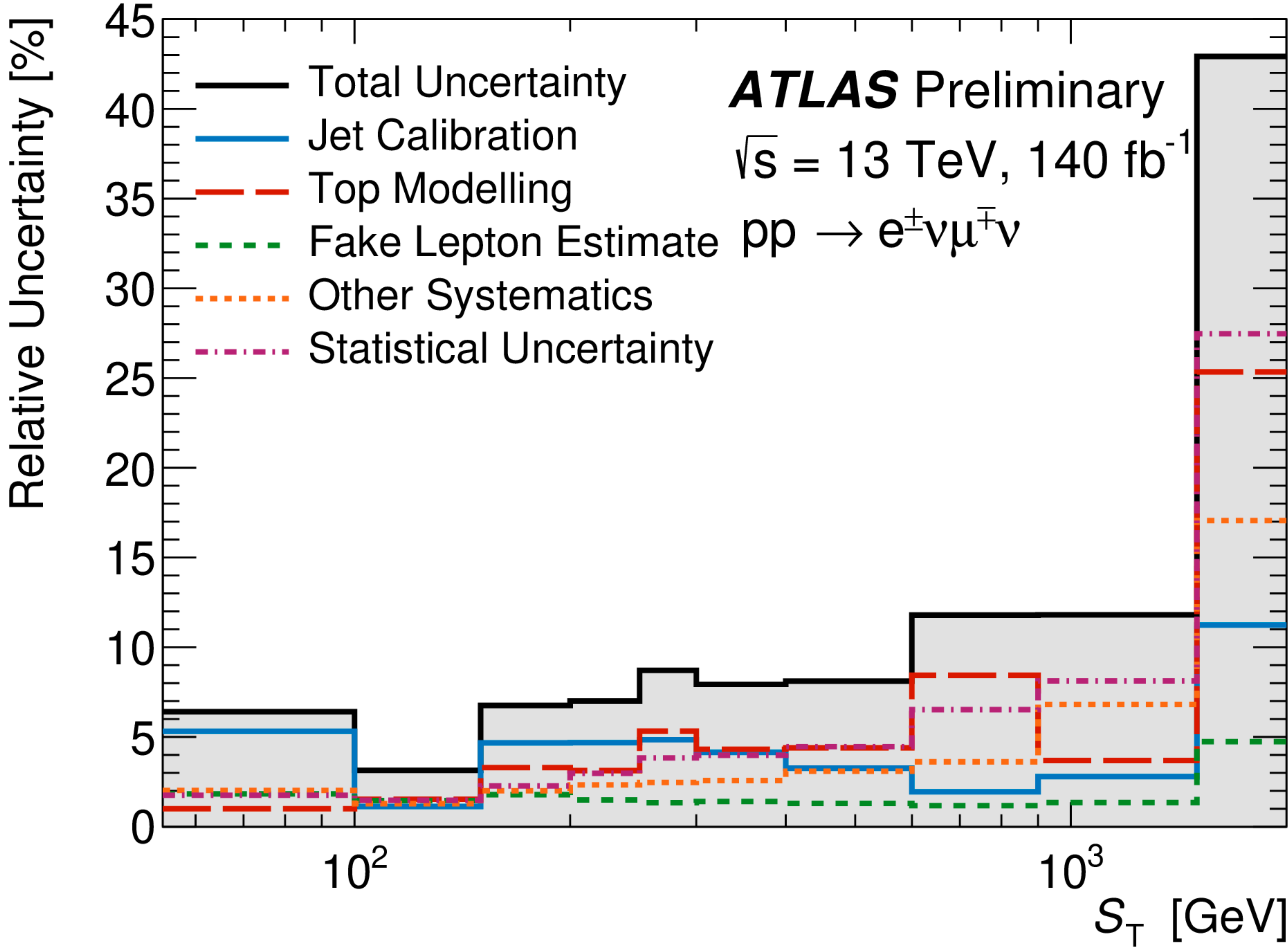

Systematic uncertainties breakdown for two observables

WZ Joint Polarization

Phys. Lett. B 843 (2023) 137895

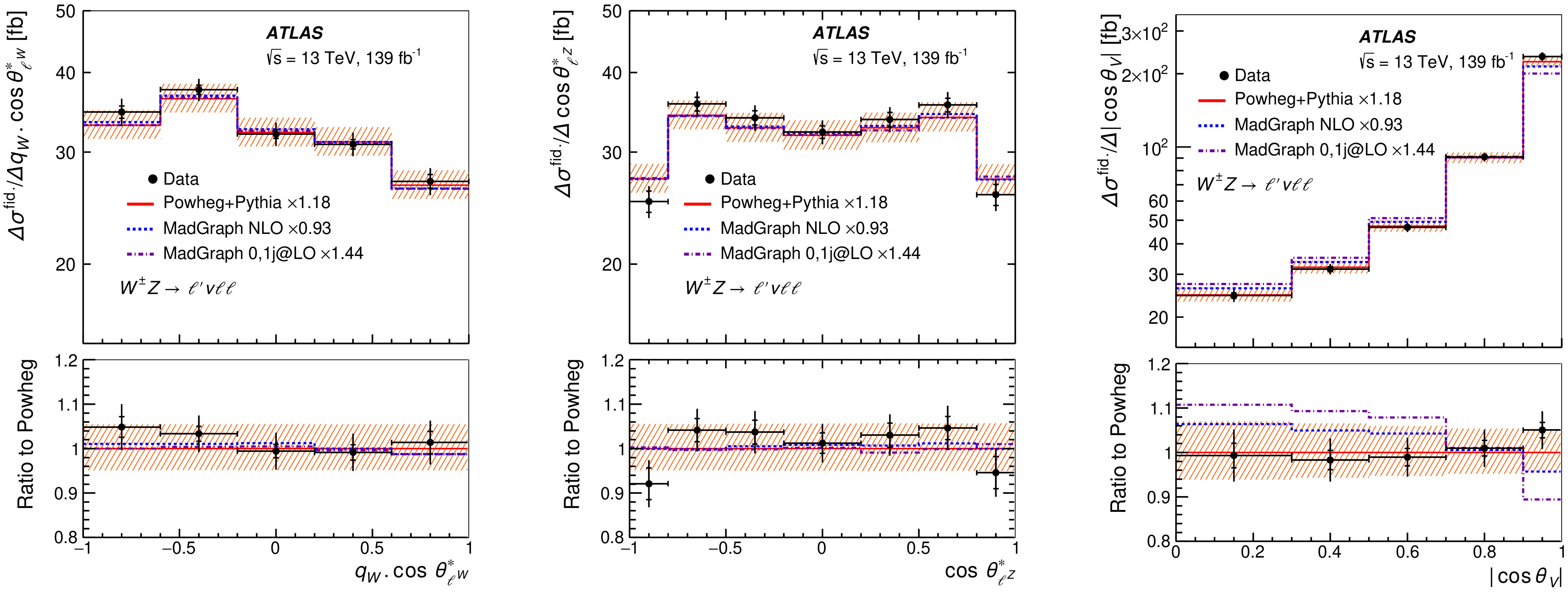

Differential XS measurements of polarization sensitive observables

WZ Joint Polarization

Phys. Lett. B 843 (2023) 137895

	Data	Powheg+Pythia	NLO QCD
$W^{\pm}Z$			
f_{00}	0.067 ± 0.010	0.0590 ± 0.0009	0.058 ± 0.002
$f_{0\mathrm{T}}$	0.110 ± 0.029	0.1515 ± 0.0017	0.159 ± 0.003
$f_{\mathrm{T}0}$	0.179 ± 0.023	0.1465 ± 0.0017	0.149 ± 0.003
f_{TT}	0.644 ± 0.032	0.6431 ± 0.0021	0.628 ± 0.004
$W^{+}Z$			
f_{00}	0.072 ± 0.016	0.0583 ± 0.0012	0.057 ± 0.002
$f_{0\mathrm{T}}$	0.119 ± 0.034	0.1484 ± 0.0022	0.155 ± 0.003
$f_{\mathrm{T}0}$	0.152 ± 0.033	0.1461 ± 0.0022	0.147 ± 0.003
f_{TT}	0.66 ± 0.04	0.6472 ± 0.0026	0.635 ± 0.004
$W^{-}Z$			
f_{00}	0.063 ± 0.016	0.0600 ± 0.0014	0.059 ± 0.002
$f_{0\mathrm{T}}$	0.11 ± 0.04	0.1560 ± 0.0027	0.166 ± 0.003
$f_{\mathrm{T}0}$	0.21 ± 0.04	0.1470 ± 0.0027	0.152 ± 0.003
f_{TT}	0.62 ± 0.05	0.6370 ± 0.0033	0.618 ± 0.004

Measured joint helicity fractions

	f_0			$f_{\mathrm{L}} - f_{\mathrm{R}}$	
	Data	Powheg+Pythia	NLO QCD	Data	Powheg+Pythia
W in $W^{+}Z$	0.23 ± 0.05	0.2044 ± 0.0024	0.211 ± 0.002	0.071 ± 0.023	0.0990 ± 0.0015
W in $W^{-}Z$	0.19 ± 0.05	0.217 ± 0.004	0.225 ± 0.001	0.026 ± 0.027	-0.0491 ± 0.0020
W in $W^{\pm}Z$	0.21 ± 0.04	0.2094 ± 0.0016	0.217 ± 0.001	0.059 ± 0.016	0.0390 ± 0.0011
Z in $W^{+}Z$	0.223 ± 0.025	0.1971 ± 0.0019	0.206 ± 0.002	-0.20 ± 0.10	-0.217 ± 0.006
Z in $W^{-}Z$	0.241 ± 0.029	0.2065 ± 0.0023	0.211 ± 0.001	0.10 ± 0.13	0.092 ± 0.007
Z in $W^{\pm}Z$	0.231 ± 0.019	0.2009 ± 0.0014	0.208 ± 0.001	-0.10 ± 0.08	-0.092 ± 0.005

Measured individual helicity fractions

WZ Production Measurement

CMS-SMP-20-014

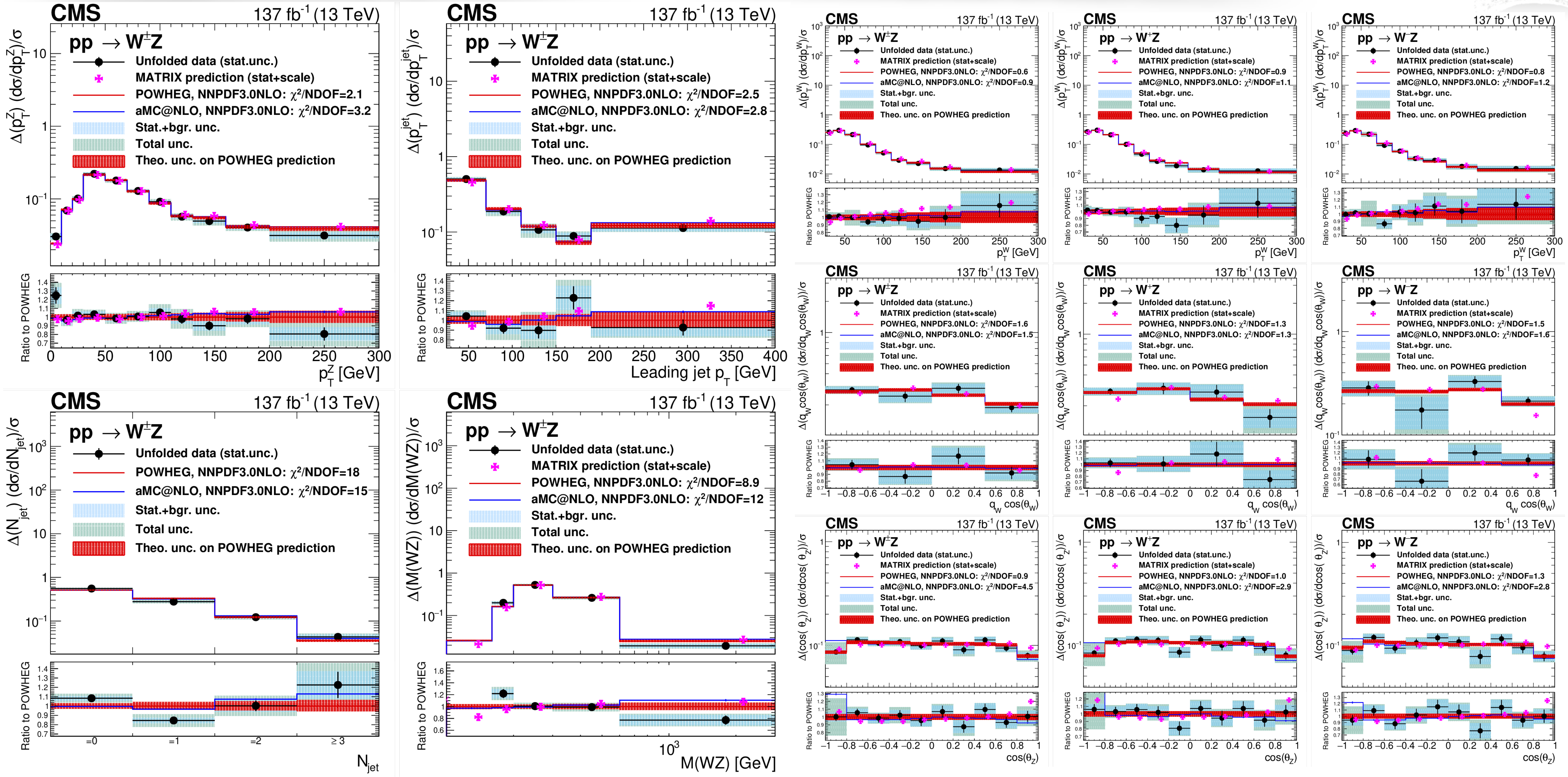

WZ Production Measurement

CMS-SMP-20-014

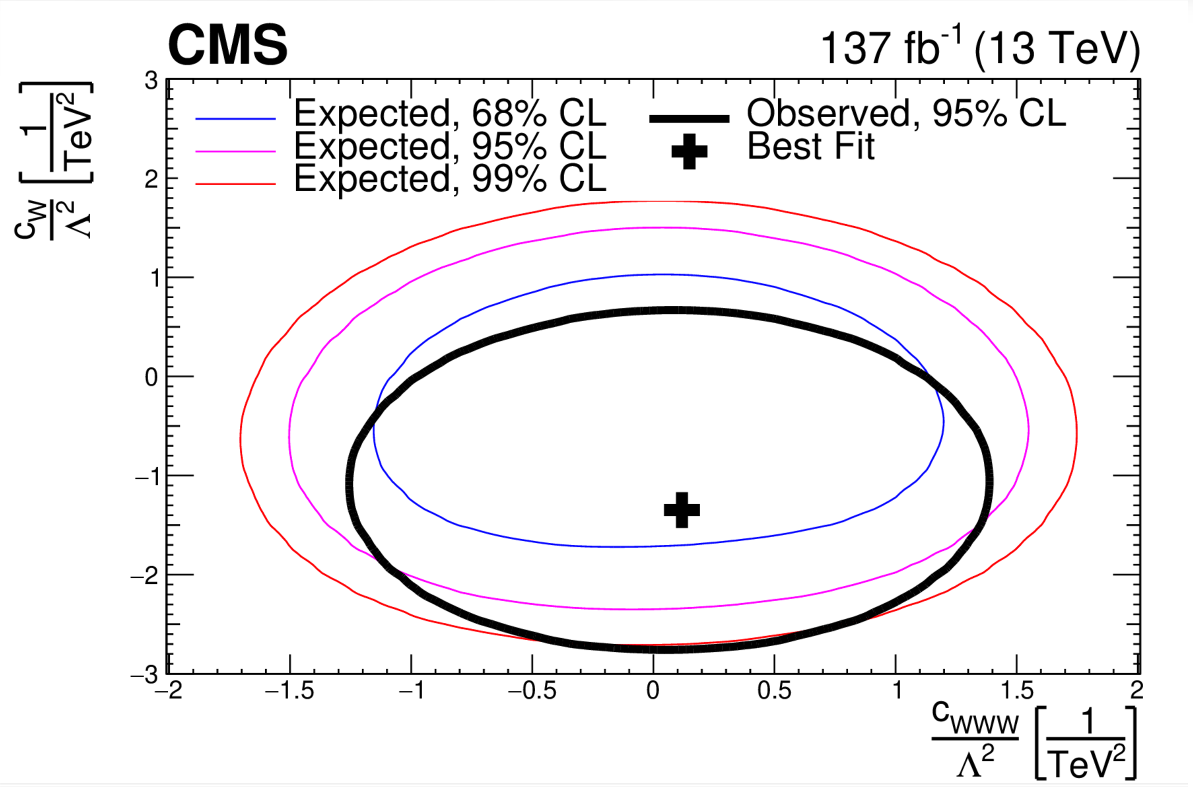

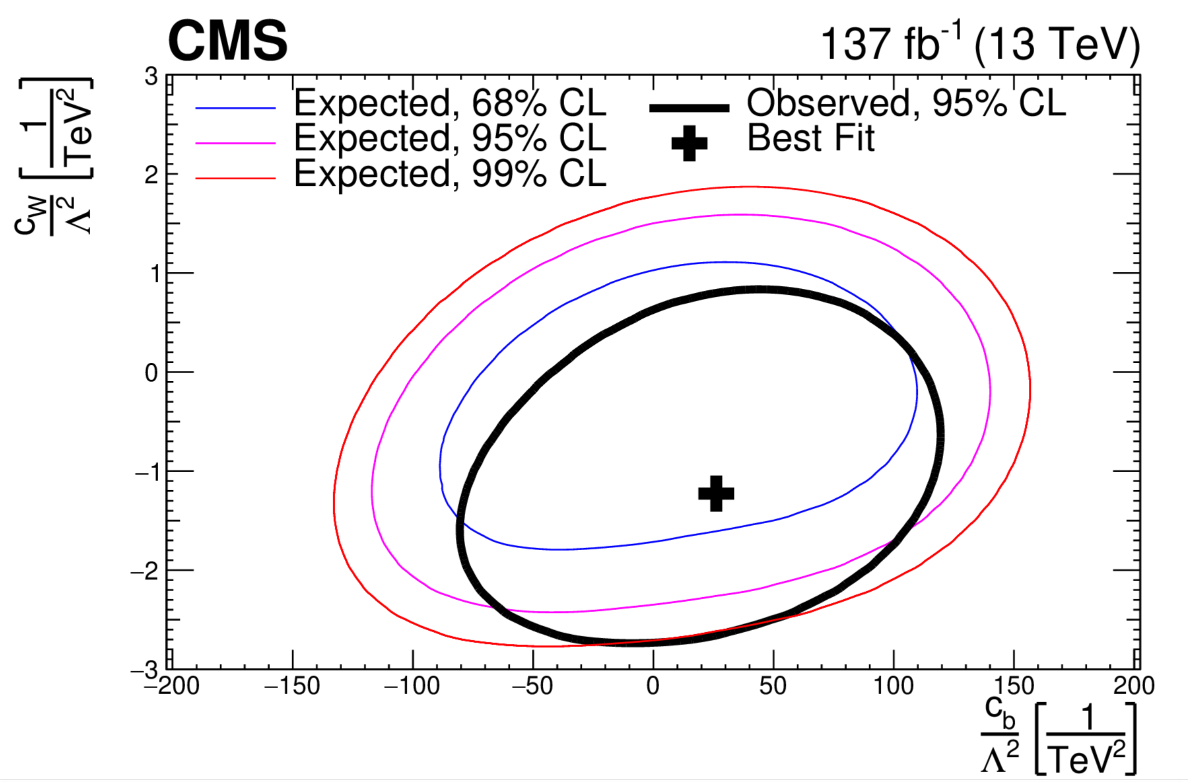

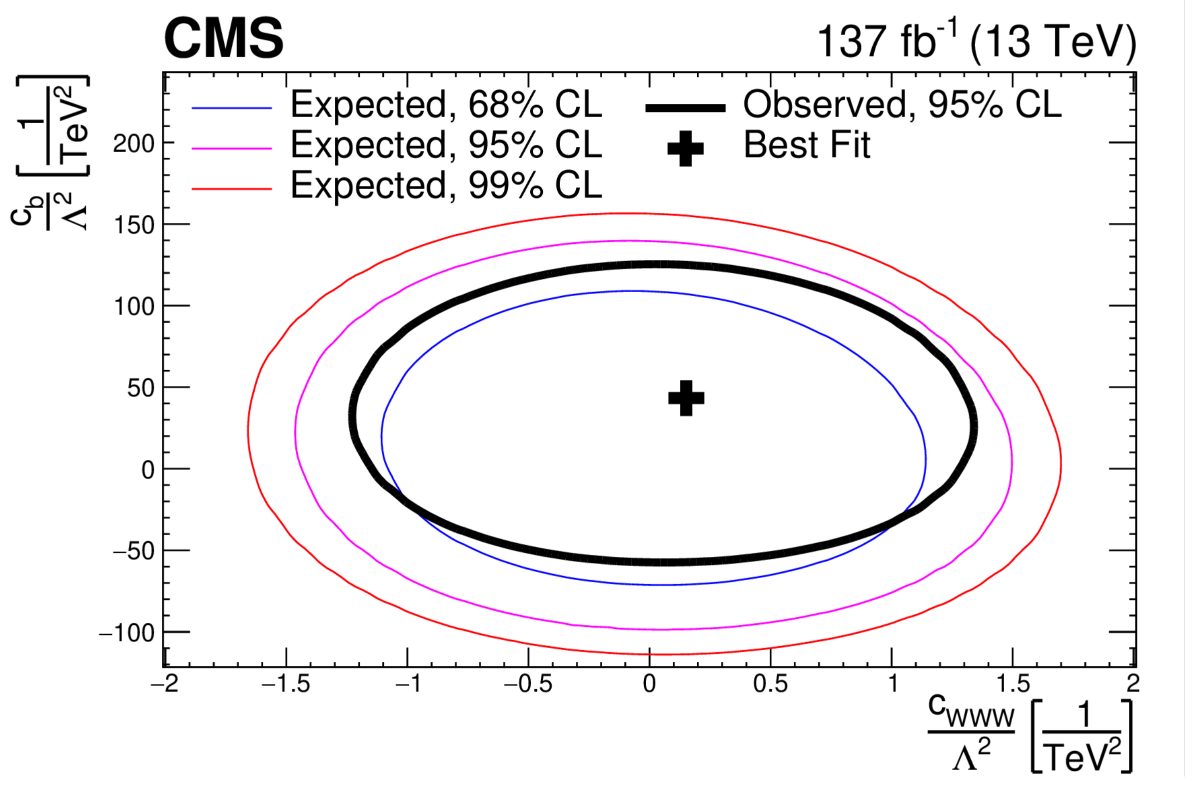

Parameter	95% CI, exp. (TeV^{-2})	95% CI, obs. (TeV^{-2})	Best fit, obs. (TeV^{-2})
c_{W}/Λ^2	$[-2.0, 1.3]$	$[-2.5, 0.3]$	-1.3
c_{WWW}/Λ^2	$[-1.3, 1.3]$	$[-1.0, 1.2]$	0.1
c_{b}/Λ^2	$[-86, 125]$	$[-43, 113]$	44
$\tilde{c}_{WWW}/\Lambda^2$	$[-0.76, 0.65]$	$[-0.62, 0.53]$	-0.03
$\tilde{c}_{W}/\Lambda^2$	$[-46, 46]$	$[-32, 32]$	0

Dimension-6 and Dimension-8 operators

Parameter	95% CI, exp. (TeV^{-2})	95% CI, obs. (TeV^{-2})	Best fit, obs. (TeV^{-2})
c_{W}/Λ^2	$[-1.8, 2.1]$	$[-3.1, 0.3]$	-1.6
c_{WWW}/Λ^2	$[-8.5, 8.5]$	$[-4.2, 14.2]$	5.5
c_{b}/Λ^2	$[-200, 180]$	$[10, 380]$	200
$\tilde{c}_{WWW}/\Lambda^2$	$[-3.3, 4.1]$	$[-4.0, 3.6]$	-0.6
$\tilde{c}_{W}/\Lambda^2$	—	—	—

Dimension-6 operators only

Zγ+Jets Differential

JHEP 07 (2023) 072

Resolution Variable: Vanish at Lead Order

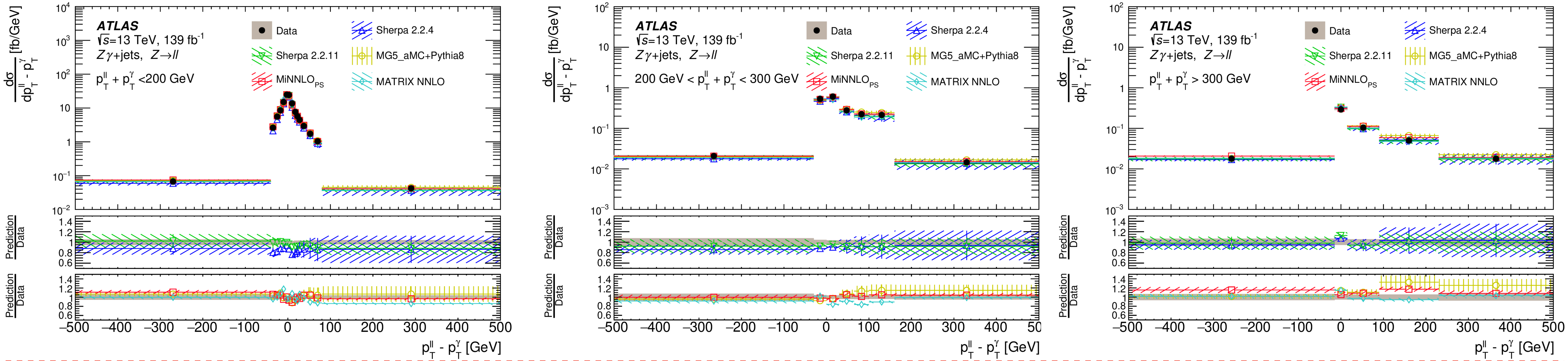

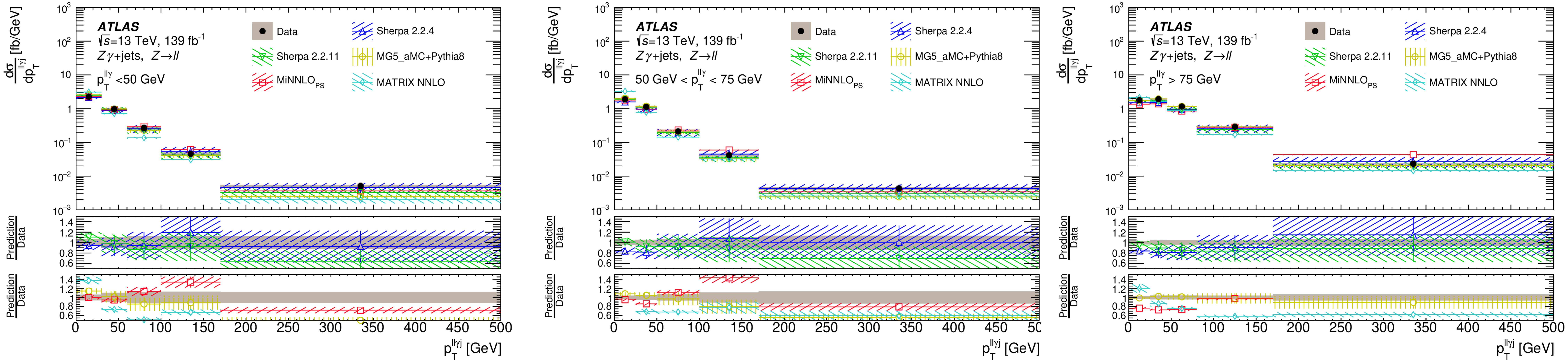

Hard variable: Non-zero at Leading Order QCD calculation

ZZ->4l Angular Analysis

ATLAS-CONF-2023-038

- **1D reweighting for each individual polarisation state.** In this step, the reweighting is done separately for the $q\bar{q} \to ZZ$ and $gg \to ZZ$ processes. For $q\bar{q} \to ZZ$, the combined NLO QCD and EW corrections as a function of the $\cos\theta_1$ variable are applied by taking the ratio of the differential cross-sections calculated from MoCaNLO at NLO and the ones from the MadGraph5_aMC@NLO MC samples at the particle level in the fiducial phase space of the measurement, for $Z_\mathrm{T}Z_\mathrm{T}$, $Z_\mathrm{T}Z_\mathrm{L}$ and $Z_\mathrm{L}Z_\mathrm{L}$ events, respectively. An additional reweighting as a function of $\cos\theta_1$ is applied to account for the missing higher-order QCD and parton shower effects by taking the ratio of unpolarised Sherpa $q\bar{q} \to ZZ$ predictions at the particle level to the unpolarised MoCaNLO calculations. The impact of these two 1D reweighting corrections on the BDT discriminant is mostly on the normalisation, about 20%, and the shape variation is 2 – 4%. For $gg \to ZZ$, which contributes to about 15% of the total signal yield, only the unpolarised MadGraph5_aMC@NLO MC sample at LO is available, and the MoCaNLO program provides polarised differential cross-sections at LO. Thus the unpolarised MadGraph5_aMC@NLO MC sample is reweighted to obtain polarised templates of $Z_\mathrm{T}Z_\mathrm{T}$, $Z_\mathrm{T}Z_\mathrm{L}$ and $Z_\mathrm{L}Z_\mathrm{L}$, by taking the fraction of polarised and unpolarised cross-sections calculated by MoCaNLO as a function of $\cos\theta_1$.
- **1D reweighting for the interference effect.** The simulated polarised samples does not consider the interference effects among different polarisation states, while such interference effects are found to be non-negligible in some kinematic regions where the contribution could reach up to 5% [66]. A dedicated template for the interference term is therefore constructed by reweighting the unpolarised Sherpa $q\bar{q} \to ZZ$ events with MoCaNLO calculations that include interference contributions, by taking the difference between the unpolarised cross-sections and the sum of the three polarised cross-sections as a function of $\cos\theta_1$. For $gg \to ZZ$ events, the interference effect is found to be negligible and thus ignored. For the subleading EW $qq \to ZZjj$ process, the interference effect is not included either.
- **2D reweighting for the residual higher-order corrections.** Four templates, including three polarisation states and the interference term, are obtained after the two reweighting steps described above. A closure test is performed by comparing the sum of the four templates and the prediction given by the unpolarised Sherpa MC events and residual discrepancies are observed, which could be due to the non-closure of the 1D reweighting method. An additional 2D reweighting is applied to each of the three polarisation templates to correct the mismodelling by taking the ratio of the non-closure effect and the sum of the three polarisation templates as a function of $\cos\theta^*_{Z_1}$ and $\Delta\phi_{\ell_1\ell_2}$. The impact of this 2D reweighting on the BDT discriminant is mostly on the shape with a variation of about 10%.

Reweighing of signal polarization samples

The OO defined for the CP study combines the CP-sensitive polar and azimuthal angles of both Z boson systems, providing additional CP sensitivity from shape differences between the SM and aNTGC predictions. The CP-sensitive polar angles $\theta_1(\theta_3)$ for the $Z_1(Z_2)$ boson are already defined in Section 6.1. The CP-sensitive azimuthal angles ϕ_1 and ϕ_3 are reconstructed in a reference frame that allows a direct measure of the Z boson spin as discussed in Ref. [24, 89] and are illustrated in Figure 2. The CP-sensitive azimuthal angle $\phi_1(\phi_3)$ is the azimuthal angle of the negative lepton in the $Z_1(Z_2)$ rest frame in this new axis system. The differential cross-sections for $\theta_1(\theta_3)$ and $\phi_1(\phi_3)$ are symmetric in the SM but asymmetric in the presence of the two CP-odd aNTGC.

To improve the sensitivity, the two CP-sensitive angles $\theta_1(\theta_3)$ and $\phi_1(\phi_3)$ are combined to form an angular observable $T_{yz,1(3)} = \sin\phi_{1(3)} \times \cos\theta_{1(3)}$ which maximises the asymmetry for each Z boson system. Figures 4(a) and 4(b) show the 2D differential distributions of the CP-sensitive observable T_{yz} of the two Z bosons, the symmetric SM prediction and asymmetric BSM prediction in the presence of a non-zero f^4_Z parameter.

As observed in Figure 4(b), the first (bottom left) and the third (top right) quadrants where both Z bosons have negative and positive T_{yz} values, respectively, are the most sensitive regions of the 2D T_{yz} distribution. The OO $O_{T_{yz,1},T_{yz,3}}$ is defined from the $2D$ distribution of T_{yz} by grouping together the sensitive and non-sensitive bins to maximise the sensitivity for the four-lepton system. Each bin of the $O_{T_{yz,1},T_{yz,3}}$ observable represents approximately an L-shaped grouping of the bins around $T_{yz,3} = T_{yz,1}$ line as shown by Figure 5(a). The small fraction of events with miss-paired leptons in the $ZZ \to 4e$ (4μ) final states were studied and found to have negligible impact on the CP-sensitivity of the OO.

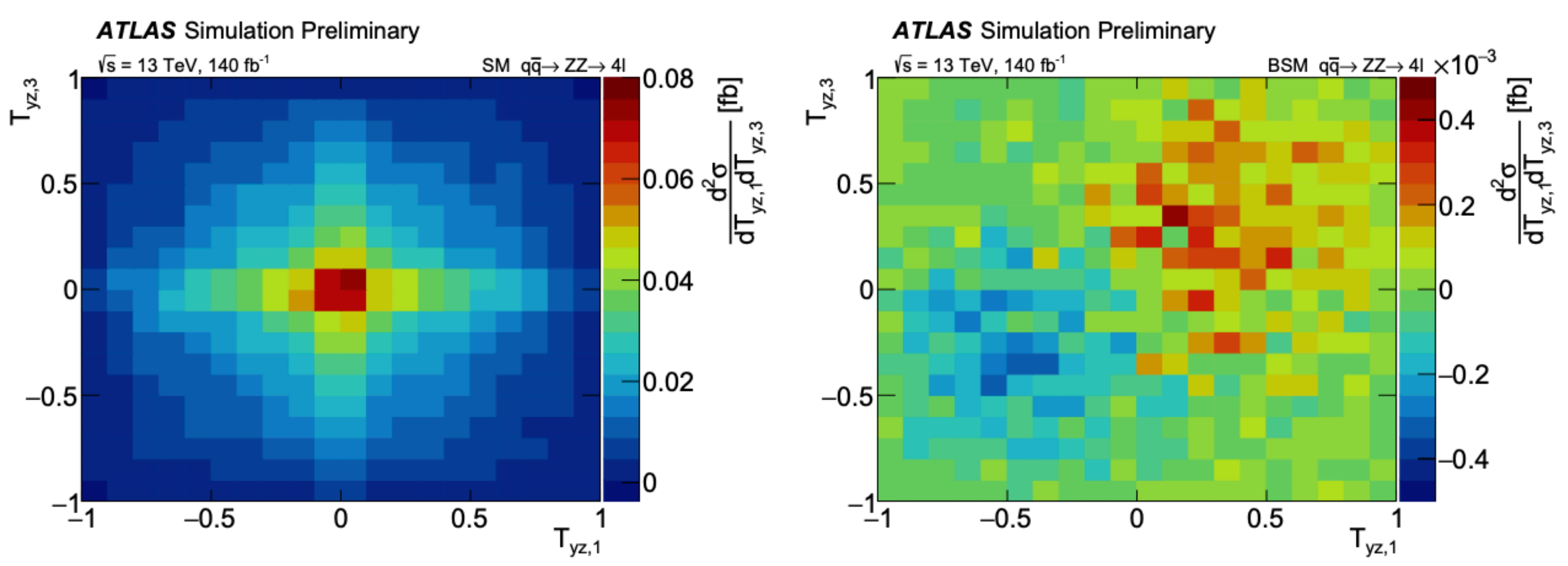

(a) (b)

Figure 4: Particle level 2D differential cross-sections of T_{yz} of the two Z bosons for the $q\bar{q} \to ZZ \to 4\ell$ process as predicted by (a) the SM and (b) in the presence of the BSM aNTGC vertex. The BSM prediction shows the linear only contribution when $f^4_Z = 1$.

Definition of CP-odd observable

Search for γγ->VV

CMS-SMP-21-014

5.4 Proton-jet matching and signal region

The matching between the proton and jet kinematics for exclusive signal is based on the variables $1 - m(\mathrm{VV})/m(\mathrm{pp})$ and $y(\mathrm{pp}) - y(\mathrm{VV})$. Here $m(\mathrm{VV})$ and $y(\mathrm{VV})$ represent the invariant mass and rapidity of the WW or ZZ system, as reconstructed from the merged jets. The variables $m(\mathrm{pp})$ and $y(\mathrm{pp})$ are the expected invariant mass and rapidity of the central system, calculated from the proton information:

$$m(\mathrm{pp}) = \sqrt{s}\sqrt{\xi_{\mathrm{p1}}\xi_{\mathrm{p2}}}, \qquad y(\mathrm{pp}) = -\frac{1}{2}\ln\left(\frac{\xi_{\mathrm{p1}}}{\xi_{\mathrm{p2}}}\right). \tag{2}$$

Two signal regions are defined by comparing the invariant mass and rapidity of the WW or ZZ system obtained from the jets with the same quantities inferred from the two protons. A diamond-shaped area in the $y(\mathrm{pp}) - y(\mathrm{VV})$ vs. $1 - m(\mathrm{VV})/m(\mathrm{pp})$ plane, centered around zero, contains the bulk of the signal when both protons are correctly associated to the jets ("region δ"). In case one of the signal protons is missed and a pileup proton is used instead, the events tend to fall in one of the two diagonal bands of Fig. 4. A second signal region ("region o") is therefore defined based on these bands. The dimensions of the two regions are optimized to provide the best expected signal significance, estimated as $S/\sqrt{B}$. Of the simulated signal events passing all other selections, typically between 19% and 25% are contained in region δ, and a similar fraction in region o. The area with $|1 - m(\mathrm{VV})/m(\mathrm{pp})| < 1.0$ and $|y(\mathrm{pp}) - y(\mathrm{VV})| < 0.5$, encompassing both signal regions, remained blinded and was not examined until the selection criteria and background estimation methods were fixed.

Forward protons are reconstructed using a "multi-RP" algorithm, which combines tracks reconstructed in both of the tracking Roman pots in each arm of PPS. The lever arm between the two RPs allows the reconstruction of the proton scattering angles θ^* (where the superscript "*" indicates an angle defined at the IP) and proton fractional momentum loss ξ:

$$\xi = (p_{\mathrm{nom}} - p)/p_{\mathrm{nom}}, \tag{1}$$

where p_{nom} and p are the nominal beam momentum and the scattered proton momentum,

Jet-proton matching

Dimension-8 operator: $a_0^{\mathrm{W}} = -\frac{m_{\mathrm{W}}}{\pi\alpha_{\mathrm{em}}}\left[s_w^2\frac{f_{M,0}}{\Lambda^2} + 2c_w^2\frac{f_{M,2}}{\Lambda^2} + s_w c_w\frac{f_{M,4}}{\Lambda^2}\right]$.

Table 4: Conversion of limits on a_0^{W} to dimension-8 $f_{M,i}$ operators, using the assumption of vanishing WWZγ couplings to eliminate some parameters. When quoting limits on one of the operators, the other is fixed to zero. The results for $|f_{M,0}/\Lambda^4|$ and $|f_{M,4}/\Lambda^4|$ are shown with and without clipping of the signal model at 1.4 TeV, when the other parameter is fixed to the SM value of zero.

Coupling	Observed (expected) 95% CL upper limit No clipping	Observed (expected) 95% CL upper limit Clipping at 1.4 TeV
$\lvert f_{M,0}/\Lambda^4\rvert$	16.2 (14.7) TeV^{-4}	19.5 (19.2) TeV^{-4}
$\lvert f_{M,4}/\Lambda^4\rvert$	90.9 (82.6) TeV^{-4}	110 (108) TeV^{-4}

Table 5: Conversion of limits on a_0^{W} and a_C^{W} to dimension-8 $f_{M,i}$ operators, using the assumption that all $f_{M,i}$ except one are equal to zero. The results are shown with and without clipping of the signal model at 1.4 TeV.

Coupling	Observed (expected) 95% CL upper limit No clipping	Observed (expected) 95% CL upper limit Clipping at 1.4 TeV
$\lvert f_{M,0}/\Lambda^4\rvert$	66.0 (60.0) TeV^{-4}	79.8 (78.2) TeV^{-4}
$\lvert f_{M,1}/\Lambda^4\rvert$	245.5 (214.8) TeV^{-4}	306.8 (306.8) TeV^{-4}
$\lvert f_{M,2}/\Lambda^4\rvert$	9.8 (9.0) TeV^{-4}	11.9 (11.8) TeV^{-4}
$\lvert f_{M,3}/\Lambda^4\rvert$	73.0 (64.6) TeV^{-4}	91.3 (92.3) TeV^{-4}
$\lvert f_{M,4}/\Lambda^4\rvert$	36.0 (32.9) TeV^{-4}	43.5 (42.9) TeV^{-4}
$\lvert f_{M,5}/\Lambda^4\rvert$	67.0 (58.9) TeV^{-4}	83.7 (84.1) TeV^{-4}
$\lvert f_{M,7}/\Lambda^4\rvert$	490.9 (429.6) TeV^{-4}	613.7 (613.7) TeV^{-4}